1	Functional classification of noncoding RNAs associated with distinct
2	histone modifications by PIRCh-seq
3	
4	Jingwen Fang ^{1, *} , Qing Ma ^{2, *} , Ci Chu ² , Beibei Huang ¹ , Lingjie Li ² , Pengfei Cai ¹ , Pedro J.
5	Batista ^{2,4} , Karen Erisse Martin Tolentino ² , Jin Xu ² , Rui Li ² , Pengcheng Du ¹ , Kun Qu ^{1, #} ,
6	Howard Y. Chang ^{2, 3, #}
7	
8	Affiliation:
9	
10	¹ Division of Molecular Medicine, Hefei National Laboratory for Physical Sciences at
11	Microscale, the CAS Key Laboratory of Innate Immunity and Chronic Disease, CAS
12	Center for Excellence in Molecular Cell Sciences, School of Life Sciences, University of
13	Science and Technology of China, Hefei, 230027, China.
14	² Center for Personal Dynamic Regulomes and Program in Epithelial Biology, Stanford
15	University School of Medicine, Stanford, CA 94305, USA.
16	³ Howard Hughes Medical Institute, Stanford University, Stanford, CA 94305, USA.
17	⁴ Present Address: Center for Cancer Research, National Cancer Institute, Bethesda, MD,
18	20892.
19	
20	*Co-first authors.
21	
22	Correspondence: H.Y.C. (howchang@stanford.edu) and K.Q. (<u>qukun@ustc.edu.cn</u>)
23	
24	Contact Information
25	Howard Y. Chang, MD, PhD
26	Stanford University School of Medicine
27	CCSR 2155c, 269 Campus Drive, Stanford, CA 94305-5168
28	Email: howchang@stanford.edu
29	Phone: 650-736-0306
30	Fax: 650-723-8762
31	

Fang et al. (CHANG), p. 2

32 ABSTRACT

33

34 Many long noncoding RNAs (lncRNAs) regulate gene transcription through 35 binding to histone modification complexes. Therefore, a comprehensive study of nuclear 36 RNAs in a histone modification-specific manner is critical to understand their regulatory 37 mechanisms. Here we develop a method named Profiling Interacting RNAs on Chromatin 38 by deep sequencing (PIRCh-seq), in which we profile chromatin-associated transcriptome 39 in 5 different cell types using antibodies recognizing histone H3 and 6 distinct histone 40 modifications associated with active or repressive chromatin states. PIRCh-seq identified 41 chromatin-associated RNAs with substantially less contamination by nascent transcripts, 42 as compared to existing methods. We classified chromatin-enriched lncRNAs into 6 43 functional groups based on the patterns of their association with specific histone 44 modifications. LncRNAs were enriched with different chromatin modifications in 45 different cell types, suggesting lncRNAs' regulation may also be cell type-specific. By integrating profiles of RNA secondary structure and RNA m⁶A modification, we found 46 47 that RNA bases which bind to chromatin tend to be more single stranded. We discovered 48 hundreds of allele-specific RNA-chromatin interactions, nominating specific single 49 nucleotide variants that alter RNA association with chromatin. These results provide a 50 unique resource to globally study the functions of chromatin-associated lncRNAs and 51 elucidate the basic mechanisms of chromatin-RNA interaction.

52

53 INTRODUCTION

54

55 RNAs are both the product of transcription and major regulators of the transcriptional process. In particular, long noncoding RNAs (lncRNAs) are numerous in 56 eukaryotes and function in many cases as transcription regulators^{1,2,3}. With the 57 development of next-generation sequencing (NGS), tens of thousands of lncRNAs have 58 been revealed in both murine and human genomes, and have emerged as important 59 regulators for different biological processes^{4,5}. However, among all expressed lncRNAs, 60 only a small subset are shown to be cell essential⁶ or important for development⁷ or 61 immune responses⁸. Strategies to annotate biochemical properties of lncRNAs will be 62 63 helpful to prioritize lncRNA candidates for functional analyses. Some well-studied cases have indicated that one major mechanism of lncRNAs is their ability to function through 64 binding to histone-modifying complexes^{9,10}. LncRNAs can either recruit chromatin 65 modifiers to regulate the chromatin states or directly regulate the process of transcription 66 through chromosome looping to bridge distal enhancer elements to promoters^{11,12}. 67 Thereby, a genome-wide identification of chromatin-associated lncRNAs may reveal 68 69 functions and mechanisms of lncRNAs in mediating chromatin modification and regulating gene transcription. 70

71

72 A considerable amount of literature has been published concerning protein-RNA interactions. The advent of technologies such as RIP¹³, CLIP¹⁴ and fRIP¹⁵ have led to the 73 discovery of multiple protein-associated RNAs, including many chromatin regulators. 74 75 Conversely, nuclear extraction methods followed by RNA-seq have enabled the detection of lncRNAs which are physically associated with chromatin¹⁶⁻¹⁸. In addition, more 76 recently reported methods like GRID-seq¹⁹, MARGI²⁰, and SPRITE²¹ can be used to 77 78 capture pair-wise RNA interactions with DNA. However, these approaches are not 79 capable of revealing which chromatin modifications are associated with specific 80 lncRNAs, and are thus limited in the ability to elucidate their potential regulatory 81 functions. For instance, a large number of lncRNAs are associated with Polycomb 82 Repressive Complex 2 (PRC2), a key mammalian epigenetic regulator, to silence gene 83 transcription by targeting its genomic loci and trimethylating histone H3 lysine 27 (H3K27me3)²². Therefore, lncRNAs associated with PRC2 complex may be enriched on 84 85 heterochromatin regions with H3K27me3 modification. On the other hand, a new class of 86 lncRNAs called super-lncRNAs were recently characterized. These lncRNAs target super-enhancers which have potential to regulate enhancer activities and transcription²³. 87 These super-lncRNAs may be enriched on euchromatin and active DNA regulatory 88 89 elements with histone H3 lysine 27 acetylation (H3K27ac), H3 lysine 4 monomethylation 90 (H3K4me1) and trimethylation (H3K4me3). Therefore, we believe it will be helpful to 91 develop an experimental technology to distinguish different histone modification-92 associated lncRNAs, as well as analytical approaches to classify them and predict lncRNA functions based on their chromatin association patterns. Another technical 93 challenge in studying chromatin associated lncRNAs is avoiding interference from 94 95 abundant nascent transcripts on chromatin. For example, results from GRID-seq¹⁹ or MARGI²⁰, approaches recently developed to identify in situ global RNA interactions with 96 DNA, contain significant amounts of nascent transcripts, making it difficult to distinguish 97 98 whether the detected RNA is truly chromatin-associated or merely captured during the 99 process of transcription.

100

101 To address these questions, we developed a new method named Profiling 102 Interacting RNAs on Chromatin followed by deep sequencing (PIRCh-seq), which 103 enriches chromatin associated RNAs in a histone modification-specific manner and 104 classifies functional lncRNAs based on the patterns of their attachment to nucleosomes 105 with specific chemical modifications. Compared to current techniques for detecting 106 chromatin-RNA association, PIRCh-seq efficiently reduces the influence of nascent 107 transcripts with a significantly lower number of intronic reads. Through performing PIRCh-seq with histone H3 and a number of different histone modification antibodies on 108 109 different cell types, we identified cell type-specific relationships between lncRNAs and 110 epigenetics. We found that chromatin-associated lncRNAs can be classified into 6 111 functional groups based on their association with chromatin modifications, which

Fang et al. (CHANG), p. 4

112 undergo dynamic changes with cell differentiation. In addition, we found that bases on 113 lncRNAs attached to chromatin tend to be more single stranded in an allele-specific 114 manner. Overall, our PIRCh-seq data provides novel insights into global functional and 115 mechanistic studies of chromatin-associated lncRNAs.

116

117 **RESULTS**

118

119 PIRCh-seq identifies RNA association with specific histone modifications in living120 cells

121

122 We conceived of PIRCh-seq as the inverse of ChIRP, a previously developed and robust method to crosslink endogenous RNA-chromatin interactions in living cells²⁴. In 123 the PIRCh-seq work flow, living cells are chemically crosslinked by glutaraldehyde and 124 125 quenched with glycine, which prevents chromatin-associated RNA from further 126 degradation. Chromatin is extracted and sonicated to 300-2000 basepair (bp) size, and 127 then immunoprecipitated (IP) by histone modification-specific antibodies. Residual DNA and proteins are removed, and retrieved RNAs are then subjected to deep sequencing 128 (Figure 1A). We tested the possibility that glutaraldehyde crosslinking may alter the 129 pull-down specificity of antibodies targeting histone modification. Using SNAP-ChIP²⁵, a 130 pool of modified mono-nucleosomes with known histone tail modifications individually 131 132 tagged with DNA barcodes, we found that glutaraldehyde crosslinking did not affect 133 antibody specificity (Figure S1A-C). The input control for PIRCh is the lysate obtained 134 after crosslinking and sonication but not subject to IP, which we also analyzed deep 135 sequencing. RNAs that are retrieved by a histone modification over input beyond that 136 expected by chance are considered PIRCh-seq hits. In this study, we generated and analyzed 26 high-resolution PIRCh-seq datasets from 2 different species: human and 137 138 mouse; 5 cell types: human H9 embryonic stem cells (H9), human female fibroblasts 139 (HFF), mouse V6.5 embryonic stem cells (mESC), mouse embryonic fibroblasts (MEF), 140 and mouse neuronal precursor cells (NPC), targeting histone H3 and 6 histone modifications (namely H3K4me1, H3K4me3, H3K27ac, H3K27me3, H3K9me3 and 141 142 H4K16ac) and input as control with 2 replicates for each experiment (Figure S1D). The expression distributions of the input RNAs extracted from our study were similar to that 143 144 of the RNAs from nuclear extraction, but differed from cytoplasmic and total RNA (data obtained from GSE57231 & GSE32916 in the same cell line) (Figure S1E), suggesting 145 146 that our chosen input could serve as a reasonable baseline for chromatin-associated RNA 147 identification. Correlation analysis of these samples indicates the high reproducibility of 148 PIRCh-seq experiments (*R*=0.900-0.988, Figure S1F-M).

149

As a proof of principle, we first examined PIRCh-seq signal of the wellcharacterized lncRNA *XIST*, which coats the inactive X chromosome in female cells, and

is known to be associated with heterochromatin with repressive histone modifications²⁶. 152 153 Indeed, we observed that the PIRCh-seq signal of XIST is highly enriched on histone H3 154 over input in human female fibroblast cells (Figure 1B), as was histone H3 PIRCh 155 followed by qRT-PCR for Xist in female murine neural stem cells (NSCs) and intact adult 156 brain (Figure 1C). These results suggest that PIRCh-seq is not only capable of enriching 157 chromatin-associated lncRNAs, but may be applied to study brain tissue in vivo. 158 Similarly, the lncRNA KCNQ10T1, which is involved in imprinting in Beckwith-159 Wiedemann syndrome by silencing lineage-specific transcription through chromatin regulation²⁷, is also enriched on histone H3 over input, as expected (Figure S2A). 160 Additionally, the imprinted oncofetal lncRNA $H19^{28}$ was also enriched by histone H3 161 162 PIRCh-seq (Figure S2B). On the other hand, abundant protein-coding and house-keeping mRNAs, such as ACTB or EEF2, did not show PIRCh-seq enrichment as expected for 163 164 cytoplasmic mRNAs (Figure S2C-D).

165

166 Next, we checked whether PIRCh-seq could enrich for RNAs associated with specific histone modifications. We performed PIRCh-seq on female NPCs with 3 167 168 ENCODE consortium validated antibodies targeting H3K4me3, H4K27ac and H3K27me3. PIRCh-seq in female NPCs demonstrated that Xist RNA was enriched by 169 170 H3K27me3, a repressive mark enriched on the inactive X-chromosome, but not by active 171 histone marks H3K4me3 nor H3K27ac that are depleted on the inactive X (Figure 1D). 172 Interestingly, from Xist's PIRCh-seq signal it is possible to infer which domain of this 173 lncRNA is associated with chromatin. Within the Xist locus, the 5' domain of Xist 174 displays significantly more substantial enrichment in H3K27me3 PIRCh-seq as compared 175 to other regions along the RNA (highlighted by the gray box, **Figure 1D**), consistent with previous findings that this is the domain potentially associated with chromatin (repC 176 domain)^{29,30,31}. Conversely, coding genes such as *Actb* and *Eef2* were not enriched on 177 178 chromatin with the same set of modifications (Figure S2E-F). These results were 179 obtained from 3 different cell lines in 2 species and indicate that PIRCh-seq is able to 180 identify histone modification specific chromatin-associated lncRNAs transcriptome-wide. 181

182 PIRCh-seq can also be utilized to identify novel histone modification-specific chromatin-enriched lncRNAs. In our NPC PIRCh-seq, a lncRNA upstream of the Nr2f1 183 184 gene, *lnc-Nr2f1*, was retrieved by the promoter marks histone H3K4me3 (P<0.05), but not enhancer-associated nor repressive modifications (H3K27ac and H3K27me3), 185 186 indicating that this lncRNA may preferentially associate with H3K4me3 regions (Figure **1E**). Recently, *lnc-Nr2f1* was reported to play a critical role in regulating 187 neurodevelopmental disorders³². In order to further validate the chromatin-RNA 188 association of this lncRNA, we retrieved *lnc-Nr2f1* RNA and mapped its associated DNA 189 190 elements in NPCs (ChIRP-seq experiment). Overlaying *lnc-Nr2f1* ChIRP-seq with ChIP-191 seq data of the histone modifications confirmed that *lnc-Nr2f1* does bind to genomic

Fang et al. (CHANG), p. 6

locations with H3K4me3 (Figure 1F-G), further confirms that the PIRCh approach can 192 193 retrieve lncRNAs specifically associated with certain modifications. In addition, gene 194 ontology analysis of *lnc-Nr2f1* ChIRP-seq peaks using GREAT³³ suggests that *lnc-Nr2f1* regulates cerebellar cortex development (Figure S2G, $P < 10^{-5}$), consistent with previous 195 findings regarding the function of this lncRNA. These results not only demonstrate the 196 197 reliability of PIRCh-seq in identifying chromatin-associated ncRNAs, but also suggest 198 potential application of the histone modification-specific PIRCh-seq approach in 199 predicting their functions.

- 200
- 201 202

PIRCh-seq enriches lncRNAs on chromatin with low nascent transcription

203 Various techniques have been developed to study ncRNA functions on chromatin. For instance, ChIRP²⁴, CHART³⁴, and RAP³⁵ are RNA-centric methods that profile DNA 204 binding sites genome-wide of one target RNA at a time. Many investigators have isolated 205 206 chromatin-associated RNAs from stringent nuclear or chromatin fractionation^{16,18}. In addition, recent methods such as GRID-seq and MARGI can be applied in mapping the 207 global RNA-chromatin interactome^{19,20}. Comparatively, chromatin fractionation and 208 sequencing detects chromatin-associated RNA without delineating the specific chromatin 209 210 states that specific RNAs prefer. Furthermore, proximity ligation methods predominantly 211 detect nascent RNAs co-transcriptionally tethered to chromatin by RNA polymerase, 212 confounding signals from the functional chromatin-associated ncRNAs and background 213 signal from all RNAs in the process of transcription. Thus, to evaluate the level of 214 nascent transcription from PIRCh, we compared our PIRCh-seq results in H9 and HFF with that from GRID-seq¹⁹, che-RNA isolation (named CPE "chromatin pellet extract" 215 for experiment and SNE "soluble-nuclear extract" for background control)¹⁸, and 216 chromatin-associated RNAs (CAR)¹⁶. These experiments were all performed in human 217 218 cell lines. We found that the ratios of intronic reads in PIRCh-seq profiles were 219 significantly lower than those from previously reported methods (P < 0.01, T-test), and 220 were almost comparable with input RNAseq from bulk cultured cells (Figure 2A). 221 Moreover, by averaging signals over the entire transcriptome centered by introns from all 222 the existing methods, we found PIRCh was more effective in obtaining mature RNAs 223 than extant chromatin-RNA enrichment methods, based on the higher signal over exons 224 than introns (**Figure 2B**). We obtained similar findings in other cell types and with every 225 tested histone modifications (Figure 2C, PIRCh-seq of V6.5 mouse ES cells with histone 226 H3 and 6 histone modifications). These results demonstrate that PIRCh-seq consistently 227 generates a significantly lower level of intronic reads with multiple histone modifications 228 than existing methods, and therefore is able to preserve regulatory interactions in trans 229 between lncRNAs and chromatin.

230

231 To further estimate the level of nascent transcription, we then integrated each 232 histone modification-specific PIRCh-seq profile with its corresponding ChIP-seq dataset 233 in the same cell line (V6.5 mESCs), and asked whether the PIRCh-seq signal of each 234 RNA correlated with the nearby ChIP-seq signal carrying the corresponding modification 235 (see Methods). The ChIP-seq profiles of each histone modification in mESC were 236 obtained from ENCODE. Our results suggest that there was no significant correlation 237 with these two sets of signals (Figure S3A-E), confirming that the nascent transcription 238 from PIRCh-seq is negligible. These results suggest that the majority of PIRCh-seq 239 enriched chromatin-associated RNAs are mature RNAs with introns spliced out, which 240 allows PIRCh-seq to identify more chromatin-associated RNAs with low abundance, 241 such as many ncRNAs.

- 242
- 243

PIRCh-seq identifies ncRNAs associated with specific histone modifications 244

245 Because PIRCh-seq enables transcriptome-wide annotation of chromatin-RNA 246 association, we next determined whether various types of RNA (especially coding RNAs 247 versus ncRNAs) are differentially affiliated with chromatin. We first applied the limma package³⁶ in R to normalize the RNA read counts in PIRCh-seq and input samples 248 249 (Figure S4A-B). We then defined a PIRCh enrichment score by dividing the normalized 250 read counts in PIRCh over input, and ranked all the transcripts by their enrichment scores 251 in H3 PIRCh-seq. To test whether ncRNAs were enriched on chromatin, we performed a gene set enrichment analysis (GSEA)³⁷ of the annotated coding and noncoding RNAs. 252 253 We found that ncRNAs, but not coding RNAs, were indeed highly enriched on chromatin 254 and many known ncRNAs were top ranked in terms of chromatin enrichment scores 255 (Figure 2D). Next, we performed PIRCh-seq with antibodies specific to distinct histone 256 modifications in mESCs. Similar to the enrichment on histone H3, we expect that 257 ncRNAs should be highly ranked by the average fold enrichment of the histone 258 modification-specific PIRCh-seq signal versus the corresponding input, among all the 259 expressed genes. Indeed, compared with mRNAs, we found that in most cases (22 out of 28) the average enrichment scores of the annotated lncRNAs, pre-miRNAs, snoRNAs, as 260 261 well as other ncRNAs were significantly higher on H3 and multiple histone modified 262 chromatin than coding genes (Figure 2E, P<0.05, T-test). We then checked the 263 distributions of the expressed and chromatin associated RNAs on histone H3 and chromatin with other modifications in mESCs, and found that ncRNAs were significantly 264 265 more frequent on chromatin compared with mRNAs (Figure S4C), serving as additional 266 evidence that ncRNAs are more enriched on chromatin in general. Furthermore, when we 267 defined a variation score which measured the standard deviation of the chromatin 268 association enrichment scores across each histone modification for every expressed RNA, 269 we concluded that ncRNAs are significantly more variable than mRNAs (Figure 2F, 270 P < 0.001, T-test). This suggests that non-coding transcripts are more differentially

enriched at distinct chromatin states, consistent with the potential regulatory function
divergence of lncRNAs, and naturally prioritizes downstream studies of lncRNAs by
activity.

274

275 We then sought to characterize the ncRNAs significantly on chromatin in mESC 276 from their PIRCh-seq profiles. We considered PIRCh-seq biological replicates versus the 277 inputs in limma³⁶ and defined an RNA with chromatin association by P-value<0.05 278 (Methods). Using this cutoff, we identified 258 chromatin associated ncRNAs in mESC 279 which were enriched in at least one of the 6 histone modification-specific PIRCh-seq 280 profiles (Table S1). To further evaluate the performance of the PIRCh approach, we 281 compared our PIRCh-seq enriched lncRNA results with 96 published RNA-chromatin 282 association profiles from ChIRP/CHART/RAP/GRID-seq datasets, collected by LnChrom³⁸. We found a total of 23 lncRNA, including *Xist*, *Firre*, *Rmrp*, *Tug1* and etc. 283 284 were also expressed in our mESCs. All 23 lncRNAs were positively enriched in PIRCh, 285 and 14 were significant with P < 0.05, reaffirming the sensitivity of the PIRCh approach in 286 identifying chromatin associated lncRNAs. Furthermore, we wanted to validate whether 287 the PIRCh lncRNA enrichment patterns were consistent with results obtained from 288 published orthogonal methods. We hypothesized that if a lncRNA is able to associate 289 with DNA elements marked by a specific histone modification, its genomic binding sites 290 from ChIRP/CHART/RAP/GRID-seq experiments should greatly overlap with 291 corresponding ChIP-seq peaks associated with the same modification. We then obtained 292 the genomic binding sites (peaks) of the 23 lncRNAs from the aforementioned 293 experiments, and found the ratio of this overlap from published data (Figure 2G) is 294 highly correlated with the corresponding PIRCh-seq signal among most of the lncRNAs 295 (Figure 2H). The Spearman correlation coefficients of the ratio of the overlap ChIP-seq peaks³⁹ with the lncRNA's PIRCh-seq enrichment scores in the same cell line were 296 297 significantly higher than random permutations (Figure 2I, P<0.0001). These results 298 further confirm that PIRCh-seq reliably identifies chromatin associated lncRNAs.

299

300 Conversely, we hypothesized that certain ncRNAs are enriched at chromatin with 301 distinct types of DNA regulatory elements, and asked whether gene regulatory elements 302 could be naturally differentiated via chromatin-ncRNA association. We then calculated 303 the pairwise Pearson correlation of all chromatin states based on the PIRCh-seq 304 enrichment scores of 258 chromatin associated ncRNAs. It is clear that the enhancer-like 305 states (H3K27ac, H4K16ac, H3K4me1) clustered together, then the promoters 306 (H3K4me3), while the repressive histone modifications (H3K27me3, H3K9me3) were 307 grouped in a distinct cluster (Figure 2J). Interestingly, the PIRCh-seq signal of histone 308 H3 clustered closest with H3K4me1 (Pearson correlation r=0.89). We observed that 309 H3K4me1 ChIP-seq signal from the same cells as above covers three to four times the

310 genomic regions than other chromatin modifications, which may reflect the differential 311 sensitivities of the different antibodies for ChIP (Figure S4D).

- 312
- 313

3 PIRCh-seq classifies functional ncRNAs via chromatin association

314

315 Different gene regulatory elements--such as enhancers, promoters, insulators, and 316 silenced elements carry distinctive and characteristic histone and DNA modifications 317 (Figure 3A)⁴⁰. We noticed that 14-25 ncRNAs in HFF and H9 respectively were also 318 reported as "essential" ncRNAs with functions through CRISPRi screening⁶. We then hypothesized that specific modification enriched ncRNAs regulate each of these elements, 319 320 and thereby the functions of ncRNAs can be classified by their divergent chromatin 321 modification enrichment. Hence, PIRCh-seq is anticipated to classify and associate 322 ncRNAs with functions such as promoter, enhancer, silencer, or insulator etc. To test this 323 hypothesis, we analyzed 7sk, a well-known regulator of RNA polymerase II elongation 324 that resides at enhancers, promoters, and super enhancers⁴¹, consistent with its role in enhancer-promoter interactions. From 7sk ChIRP-seq data in mESC, we noticed that its 325 326 chromatin occupancy sites greatly overlapped with ChIP-seq peaks of H3K4me1, 327 H3K4me3, and H3K27ac in the same cell type (Figure 3B), confirming an active 328 function of 7sk. Consistently, PIRCh-seq signal of 7sk in mESC was also enriched at 329 chromatin carrying these three histone modifications, but depleted of repressive 330 modifications such as H3K27me3 and H3K9me3 (Figure 3C), suggesting the possibility 331 to extrapolate lncRNA function using PIRCh-seq.

332

We then analyzed all 258 PIRCh enriched ncRNAs and sought to categorize their 333 334 functions based on their PIRCh-seq signals. We found that these ncRNAs associate with chromatin in a combinatorial pattern, similar to those observed in ChIP-seq performed on 335 336 histone modifications (Figure S5A). H3K27ac, H3K4me3 and H3K4me1 were the top 3 337 most favored chromatin states that interacted with ncRNAs, consisting of 88% of the 338 enriched ncRNAs in mESC. As we know from histone ChIP-seq, instead of each individual modification, a combinatorial pattern of multiple modifications better 339 classifies the functions of DNA elements⁴². A machine learning strategy employing 340 341 hidden Markov model, named chromHMM, which automatically learns the major 342 combinatorial patterns, was applied successfully to classify DNA elements based on histone modifications^{43,44}. We then inquired if a similar strategy could be used to classify 343 344 chromatin-associated ncRNAs and examine if the functions of these ncRNAs could be 345 distinguished based on their association with histone modifications. To investigate this 346 relationship transcriptome-wide, we started from a 258 by 6 matrix of enrichment scores in mESC, where each row was an enriched ncRNA as defined above, each column was a 347 348 histone modification, and each element of the matrix represented the enrichment score of 349 the corresponding ncRNA on the specific modified chromatin (Methods). We then

applied K-means clustering on the matrix, where the number of Ks was determined by 350 the Silouette method⁴⁵. This analysis yielded 6 distinct groups of chromatin-associated 351 352 ncRNAs, which were visualized in a 2-dimensional projection of t-distributed stochastic 353 neighbor embedding (tSNE) (Figure 3D). Within these 258 chromatin associated ncRNAs, 247 are lncRNAs, and many well-studied ncRNAs, such as 7sk⁴¹, Neat1¹⁰ and 354 $Malat1^{46}$, and $Dancr^{47}$ naturally clustered into groups with distinct function. Interestingly, 355 356 14 lncRNAs were also reported to have a biological functional based on LncRNAdb⁴⁸, 357 and 8 out of 56 were predicted bivalent in mESCs (Figure S5B, odds-ratio=4.4, P<0.01, 358 Chi-square test). In addition, for each cluster we evaluated the relative contributions of 359 each histone modification based on the enrichment pattern of the chromatin associated 360 RNAs, and defined the clustered states by active promoters, heterochromatin, weak 361 promoter, strong enhancer, bivalent, and weak enhancer (Figure 3E). Overall, we 362 partially recapitulated the chromatin classifications based on chromHMM algorithm to ChIP-seq profiles⁴³. These results suggest that the chromatin association of ncRNAs can 363 364 be used to classify ncRNAs that might have functional implications.

365

366 Although tens of thousands noncoding transcripts were discovered in the past few years, only a small portion that function through chromatin organization were 367 368 consolidated. More recently, evidence has accumulated that indicates many lncRNAs may regulate gene expression in cis^{49,50}. Since the PIRCh approach cannot pinpoint the 369 370 exact binding sites of chromatin-associated lncRNAs, it does not directly predict whether 371 each lncRNA is functioning in cis or trans. Instead, PIRCh provides more information 372 about the epigenetic function of the lncRNA, in context of the histone modifications it 373 associates with. Our analysis suggests that chromatin-associated lncRNAs function both 374 in trans and cis. For example, when we calculated the nearby (+/-100Kb) coding gene 375 expression of the PIRCh clustered ncRNAs in Figure 3D, we observed that lncRNAs 376 were monotonically decreasing from the more active to more repressive groups; 377 additionally, the nearby coding gene expression of the "Active Promoter" and "Strong 378 Enhancer" lncRNA groups were significantly higher than that of the group "Repressed" 379 ncRNAs (Figure 3F, P<0.05, T-test). However, when the chromatin associated ncRNAs 380 were grouped based on their enrichment with each histone modification, no significant 381 expressional differences were observed from nearby coding gens. (Figure S5C), e.g. 382 compared H3K27me3 vs H3K27ac. No similar trends were observed in the expression patterns of the ncRNAs themselves (Figure S5D). These results not only indicate that the 383 384 chromatin-associated ncRNAs may function through a combinational pattern of the 385 histone modifications instead of an individual modification, but also favors the argument that the chromatin associated ncRNAs may function in cis in general. Nevertheless, not 386 all the lncRNAs enriched in our PIRCh experiment function in cis. When we integrated 387 388 each histone modification specific PIRCh-seq profile with its corresponding ChIP-seq

signal at the genomic loci of the chromatin-enriched ncRNAs, no statistical correlation
 was observed (Figure S3), suggest that some lncRNAs can function in trans.

391

392 Cell type-specific chromatin association of ncRNAs

393

394 It is known that ncRNAs are differentially expressed in distinct cell types and 395 perform specific cellular functions. Therefore, we sought to check whether the patterns of 396 ncRNA-chromatin association diverge in distinct mouse cell types, and how these 397 patterns contribute to their cell type-specific functions. We then performed PIRCh-seq on 398 MEF cells and analyzed the profiles in an identical fashion to the mESC data. Similar to 399 the mESC results, we observed that PIRCh-seq identified lncRNAs enriched on 400 chromatin with low nascent transcription (Figure S6A), and non-coding transcripts were 401 consistently more enriched on chromatin compared with protein coding gene in MEF 402 cells (Figure S6B-C), validating these conclusions in distinct cell types. We then 403 performed a similar enrichment analysis on MEF and NPC PIRCh-seq profiles and 404 obtained 200 and 110 chromatin associated ncRNAs respectively (P < 0.05). The 405 combinatorial patterns of the MEF enriched ncRNAs are predominantly similar to those 406 from mESC (Figure S6D-E). As a negative control, the IgG PIRCh was tested in tandem 407 with the other chromatin modification PIRCh experiments performed in MEF. 408 Differential analysis of PIRCh-groups over IgG control revealed that only 1 out of 200 409 PIRCh-enriched ncRNA over input was also enriched in IgG, evincing the high 410 specificity of our method in identifying the chromatin associated ncRNAs (Figure S6F). 411 In our analysis, a total of 458 chromatin enriched ncRNAs were identified in three cell 412 types, 20 of which were enriched in all three cell types (Figure 4A). We then calculated 413 the Pearson correlation coefficient matrix based on the enrichment scores of these 458 414 ncRNAs. Unsupervised clustering of this correlation matrix suggested that the cell type 415 specificity was the dominant factor which determines ncRNA chromatin association 416 (Figure 4B).

417

418 Embryonic stem cells are characterized by their pluripotency - the ability to give 419 rise to multiple cell types. The chromatin state in ES cells is reported to be more flexible than those of differentiated cells⁵¹. Interestingly, compared with those of the more 420 differentiated cells (MEF and NPC), the ncRNA chromatin association in mESCs showed 421 422 a higher correlation coefficient among distinct histone modifications, suggesting the 423 specificity of chromatin-associated ncRNAs in mESCs is more plastic than those in 424 differentiated cells (Figure 4B). In addition, we analyzed the percentage of enriched 425 ncRNA versus total expressed ncRNA in each cell type for every tested chromatin 426 modification, and found significantly more ncRNAs enriched on chromatin with 427 H3K9me3 in ES cells when compared with MEF (Figure 4C, P<0.05, Chi-square test), 428 but fewer on chromatin with H4K16ac. This result may reflect the joint presence of

Fang et al. (CHANG), p.12

activating and repressive histone marks on genome regions, termed bivalent⁵² and 429 trivalent chromatin domains⁵³ in ES cells. We identified ncRNAs which were associated 430 with both active and repressive histone marks consistent with bivalency, while others 431 432 associated with strictly active or repressive marks (Figure 4D). Since PIRCh-seq enabled 433 us to identify cell-type and histone modification specific ncRNA-chromatin associations, 434 we first screened for ncRNAs which were enriched at both active and repressive 435 chromatin in ES cells but only enriched in either active or repressive markers in 436 differentiated cells. We found several ncRNAs of this description. For example, ncRNA 437 uc008bcq.1 is broadly enriched in ES cells with high PIRCh-seq signals associated 438 H3K4me1, H3K4me3, H3K27me3 and H3K9me3 modifications, but enriched only on 439 active chromatin of H3K4me1 in MEF and repressive chromatin of H3K27me3 in NPC, 440 implying lineage-specific resolution of chromatin associations (Figure 4E). Interestingly, 441 there were dozens of such ncRNAs that are distinctly enriched in certain cell types. Since 442 ES cells possess a higher potential to differentiate into multiple lineages, and hence more 443 poised chromatin states, we expected more bivalent-enriched ("bi-enriched" for short) and fewer mono-enriched ncRNAs in mESC compared with more differentiated cells 444 445 such as MEF and NPC. In mESC, we found 30 bi-enriched and 33 mono-enriched 446 ncRNAs; while in MEF, we found only 8 bi-enriched but 32 mono-enriched ncRNAs; 447 lastly, in NPC, we found 2 bi-enriched and 11 mono-enriched ncRNAs (Figure 4F, P<0.01 for MEF and P<0.05 for NPC, Chi-square test). These results indicate that 448 449 ncRNAs may play distinct functional roles by either enhancing or repressing gene 450 expression or both in certain cell types, conducted by affixing to either active or 451 repressive chromatin or both.

452

453

454

Single-stranded RNA regions as candidate mediators of chromatin association

455 As a key player in the central dogma of biological regulation, RNA and its ability 456 to adopt specific structures is intimately involved in every step of gene expression. Previously, multiple approaches have been described in order to probe RNA secondary 457 structure transcriptome-wide in vitro⁵⁴ and in vivo^{31,55} in mammalian cells, revealing 458 structural principles of RNA-protein interactions. Correspondingly, we noted that RNA 459 enrichment on chromatin occurs in a domain-specific manner based on our PIRCh-seq 460 461 data. For instance, the repC domain of Xist is dramatically more enriched on chromatin carrying H3K27me3 modifications (highlighted by the gray box, Figure 1D). *Malat1* is 462 another well-studied chromatin-associated lncRNA which binds to active chromatin¹⁰. 463 464 Instead of attaching to histone proteins across the entire transcript, we noticed from the 465 H3K4me3 PIRCh-seq signal that there were certain regions on *Malat1* which were more closely associated with chromatin than the rest bases on the transcript (Figure 5A). 466 467 Interestingly, these regions tend to be single-stranded according to both 2' hydroxyl 468 acylation profiling experiments (icSHAPE data) and RNA secondary structure

Fang et al. (CHANG), p.13

predictions from RNAfold⁵⁶ (Figure 5B). This led us to investigate whether there are 469 470 structural preferences involved in RNA-chromatin association (Figure 5C). We first obtained a transcriptome-wide and per-base RNA secondary structure profile from 471 icSHAPE data measured in mESCs⁵⁵. A high icSHAPE score suggests a greater 472 probability that a base is single stranded. We then applied a 5-base sliding window 473 474 method to identify the enriched sites (peaks) on each RNA which interacted with 475 chromatin from PIRCh-seq, compared with our input control (see Methods). We then 476 overlaid the structural profiles from icSHAPE on top of all the histone modification 477 specific PIRCh-seq peaks centered by the peak summits and generated an average 478 structural profile for each modification. Our results show that bases ~5-10 nt upstream of 479 the chromatin associated peaks are more likely to be single stranded (**Figure 5D**). To test 480 the significance of this single-strand preference, we performed 2-tailed Welch's T-tests 481 by comparing all the icSHAPE scores of the bases from PIRCh-seq peaks with those 482 from a randomly selected background, and found this phenomenon was significant with 483 $P < 10^{-5}$. We then asked whether RNAs containing a greater number of single-stranded bases are more likely to be associated with chromatin. We separated expressed RNAs 484 485 into two groups based on chromatin enrichment or depletion, and calculated the average icSHAPE scores for every RNA in each group. We noticed that, on average, RNAs 486 487 enriched on chromatin tended to be more single-stranded with higher icSHAPE scores (Figure 5E, P<0.001, T-test). Similarly, we took the top 100 most single-stranded RNAs 488 489 and top 100 most double-stranded RNAs based on their average icSHAPE scores and 490 confirmed that the average chromatin enrichment scores of the most single-stranded 491 RNAs were significantly higher than those of the double-stranded RNAs (Figure 5F, 492 P < 0.01, T-test). These results suggest that RNAs containing more single stranded regions 493 are more likely to associate with chromatin.

- 494
- 495 496

Single nucleotide variants and RNA modifications that alter chromatin association

497 Genetic variation can alter RNA structure and function in vivo. Single nucleotide 498 polymorphisms (SNPs) comprise the most prevalent source of variation, and SNPs that 499 alter RNA secondary structures, termed "riboSnitches" (a fusion of SNP and riboswitch), 500 are a recently appreciated source of noncoding variants associated with human diseases⁵⁷. 501 We therefore asked whether different alleles of the same RNA may differentially 502 associate with chromatin; and if so, how is it related to the RNA structure? In order to 503 answer those questions, we performed PIRCh-seq in the NPC line that is derived from the 504 F1 hybrid offspring of two mouse parental lines (129S1 and CAST) with a high density 505 of SNPs across the genome (~1 SNP per 100 nucleotides). We first built the reference 506 genomes for each mouse line and aligned the raw reads to 129S1 and CAST separately 507 with 0 mismatches to reduce false positive hits. Reads mapped to either 129S1 or CAST 508 were counted to construct the allele-specific RNA expressions and chromatin

Fang et al. (CHANG), p.14

509 enrichments profiles (see **Methods**). First, we looked at whether allelic RNA chromatin 510 association is related to allelic expression. From allele-specific PIRCh-seq analysis, we 511 found that for most RNAs, allelic or unbiased expression from the two alleles determines 512 allelic or unbiased chromatin association pattern. For example, it is known that only the 513 129S1 version of the lncRNA Xist is expressed in this cell line. Consistent with allelic 514 expression, we found that enrichment of Xist in H3K27me3 modification is much higher 515 in 129S1 versus the CAST version of the lncRNA (Figure 5G). An additional example is 516 the lncRNA Malat1 in which both the 129S1 and CAST alleles are almost equally 517 expressed. As predicted, we observed unbiased enrichment on chromatin for both alleles. 518 Moreover, we discovered several lncRNAs that are enriched on chromatin in an allele-519 specific manner independent of the expression levels from the two alleles (Table S2). For example, Gas5 is a lncRNA that binds to PRC2 complex and mediate transcriptional 520 521 repression⁵⁸. We found that *Gas5* is enriched in H3K27me3 modification, consistent with 522 its understood repressive function. Notably, even though the CAST version of Gas5 was 523 3-fold more expressed in the input sample, the 129S1 allele was 4-fold more enriched on 524 chromatin carrying H3K27me3 modification (Figure 5G, P<0.05, T-test), suggesting that 525 129S1 allele of Gas5 preferentially associates with chromatin. To further investigate the 526 mechanism under Gas5 allele-specific enrichments, we predicted the secondary structure 527 of the 129S1 and CAST version of *Gas5* using RNAfold (Figure S7A, B), and found that 528 several riboSnitches (1774 T/C, 1804 C/T, 1810 T/A, 1812 T/G, 1887 T/C, CAST(mm9) 529 /129S1) converted one of the chromatin binding sites of Gas5 from single-stranded in 530 129S1 to double-stranded in CAST and thus depleted its association with repressive 531 chromatin in the latter (Figure 5H). Consistent with this prediction, when we calculated the icSHAPE score obtained from mESC containing 129S1 allele⁵⁹ for the *Gas5* region 532 allelic enriched in H3K27me3, we concluded that the region is more likely to be single 533 534 stranded (Figure S7C).

535

536 Another major factor that can influence RNA structure is RNA modification, such 537 as the N6-methyladenosine (m⁶A) modification. Previous studies have shown that m⁶A can alter base-pairing thermodynamics and destabilize RNA duplexes^{55,60,61}. We also 538 evaluated whether RNA modifications affect RNA-chromatin association. We integrated 539 540 PIRCh-seq data with the transcriptome-wide profiles of RNA m⁶A modifications in mESCs from our previous study⁶², and found the distribution of PIRCh-seq peaks along 541 the transcripts is similar to that of m^6A modified regions (Figure S8A). When we 542 overlaid m⁶A signals on top of PIRCh-seq peaks, we found that RNA bases associated 543 with chromatin are generally more $m^{6}A$ modified ($P < 10^{-5}$ in H3, Figure S8B-C). These 544 results may reflect that the tendency of m⁶A to induce RNA single-stranded regions that 545 coincide with elements for chromatin association, or due to additional mechanisms that 546 547 jointly impact chromatin association and RNA modification.

548

Fang et al. (CHANG), p.15

549 **DISCUSSION**

550

551 552

PIRCh-seq identifies chromatin associated RNAs genome-wide

553 A large and growing body of literature has investigated protein-RNA interactions. The development of approaches such as RIP¹³, CLIP¹⁴ and fRIP¹⁵ have enabled the 554 555 successful elucidation of many RNAs associated with proteins, including multiple 556 chromatin regulators. Studies have also shown that many lncRNAs function through 557 DNA/chromatin interaction. Previously described techniques such as ChIRP-seq and 558 CHART-seq have been used to identify genome-wide binding sites of specific lncRNA to 559 chromatin. However, these methods require prior knowledge of which particular 560 lncRNAs are capable of binding to chromatin before ChIRP-seq or CHART-seq can be 561 applied. Furthermore, ChIRP or CHART are limited to examining one chromatin 562 associated RNA at a time. In this study, we describe a new technology, PIRCh-seq, which 563 enables a global profiling of chromatin-associated RNAs through a robust method to crosslink endogenous RNA-chromatin interactions in living cells. Compared with current 564 methods which predominantly detect nascent RNAs co-transcriptionally tethered to 565 chromatin by RNA polymerase, PIRCh-seq significantly reduces the influence of nascent 566 567 transcripts, and more clearly reveals relationships between chromatin-associated ncRNAs. Although the PIRCh approach cannot pinpoint the exact binding sites of the chromatin 568 569 associated lncRNAs, and therefore does not inform whether each lncRNA is functioning 570 in cis or trans, PIRCh is able to provide a significantly higher ratio of mature RNAs and 571 thereby preserve the regulatory interactions in trans between lncRNAs and chromatin. Examples of some well-studied cases, such as Xist, 7sk, H19 and KCNQ10T1 etc. 572 573 demonstrate that PIRCh-seq is likely generalizable to the majority of ncRNA. 574 Additionally, PIRCh-seq identifies novel chromatin-associated lncRNAs and not only 575 provides potential targets for mechanistic studies using ChIRP and CHART, but could 576 also be extended to reveal the function and mechanisms of lncRNAs which are disease-577 relevant. However, the PIRCh-seq approach, like RIP/CLiP-seq like methods, may also 578 be heavily contaminated with co-purified mRNA species that often compose more that 50% 579 of RNA material. Therefore, further experimental and analytical improvements are 580 required to truly capture chromatin-associated ncRNAs.

581

582 PIRCh-seq classifies ncRNA putative function via histone modification and cell 583 type-specific chromatin-RNA association

584

585 Another major advantage of the PIRCh method is that it utilizes antibodies to pull 586 down chromatin with specific chemical modifications and thereby enables the 587 classification of chromatin-associated ncRNAs with putative functions such as promoter, 588 enhancer, silencer or bivalent. Since we performed PIRCh-seq with various histone

Fang et al. (CHANG), p.16

589 modification antibodies and in different human and murine cell types, the dataset 590 provides rich resources to study chromatin-associated ncRNAs in mammalian cells. In 591 addition, different cell types and histone modifications did not show much technical 592 variation, confirming that PIRCh-seq may be a useful technology to perform profiling of 593 epigenetic-associated ncRNAs. Analogous to the types of gene regulatory elements 594 bearing distinctive histone and DNA modifications, we developed a bioinformatics 595 method to classify the putative biological functions of ncRNAs based on their enrichment 596 patterns on chromatin with different histone modifications. Our method successfully 597 arranged several well studied lncRNAs in the correct functional category, and predicted 598 functions for hundreds of other ncRNAs from their chromatin association patterns. More 599 importantly, when a similar analysis was performed on multiple cell types, chromatin 600 state-specific ncRNA enrichment patterns were generally conserved, suggesting this is a 601 reliable method for functional classification. Since ncRNA-chromatin interaction is likely 602 a widespread epigenetic regulation mechanism in many cell types, our integrative 603 approach in identifying and classifying chromatin-associated ncRNAs can be broadly 604 applicable to many other cell types to deeper investigate ncRNA functions. However, chromatin association does not guarantee that a ncRNA will have a biological function; 605 furthermore, the histone modification specific PIRCh-seq approach can only predict 606 607 putative functions. As such, the true function of each ncRNA still requires further 608 investigation beyond PIRCh-seq.

- 609
- 610
- 611

) RNA secondary structure affects RNA-chromatin interaction

612 We observed that RNAs attach to chromatin in a domain-specific manner. 613 However, when we surveyed the enriched sites of chromatin-associated RNAs linked to various histone modifications in different cell types, we did not find significant sequence 614 615 motifs, suggesting the existence of a complex mechanism responsible for the RNA-616 chromatin interaction. On the other hand, when we integrated PIRCh-seq signals with RNA structural information from previous icSHAPE and RNA modification m⁶A profiles 617 and further evaluated structural information regarding the enriched domains, we found 618 619 that ncRNAs were likely to bind to chromatin through single-stranded region or bases 620 with m⁶A methylation. This may possibly be explained by the supposition that RNA-621 dependent recruitment of transcriptional activators and repressors may occur within a 622 double-stranded structural region, and therefore, single-stranded regions are made more 623 accessible to chromatin. In addition, chromatin interactions may also be allele-specific, 624 especially when certain alleles result in distinct RNA secondary structures. In conclusion, 625 when taken as a whole, these results open new avenues of inquiry and require further 626 investigation to fully elucidate the molecular mechanisms of ncRNA-chromatin interaction. 627

628

Fang et al. (CHANG), p.17

629 Author Contributions

630

KQ, QM, CC, HYC conceived the project. QM, CC, LL, PJB, KEMT, RL performed
PIRCh-seq library generation and qPCR experiments. JF performed all data analysis with
assistance from BH, PC, QM, JX and PD. KQ, HYC, JF, and QM wrote the manuscript
with inputs from all authors.

635

636 Data and code availability

637

The PIRCh-seq and ChIRP-seq data generated in this study can be obtained from NIH GEO with the accession number GSE119006 and is available by go to the following website <u>https://www.ncbi.nlm.nih.gov/geo/query/acc.cgi?acc=GSE119006</u>, and entering token "ulglmesubpmdbkx" in the box. Other published data sets used in this study are available and described in the Reporting Summary file. All in house developed codes/scripts were uploaded to Github website (https://github.com/QuKunLab/PIRCh).

644

645 Acknowledgments

646

647 We thank the members of Chang and Ou labs for their discussions. This work was 648 supported by the National Key R&D Program of China 2017YFA0102900 (to K.O.), the 649 National Natural Science Foundation of China grant (81788101, 91640113, 31771428 to 650 K.Q.), the Chinese Government 1000 Youth Talent Program (to K.Q.), the research start-651 up from the University of Science and Technology of China (to K.Q.); the NIH grants 652 P50-HG007735 and R01HG004361 (to. H.Y.C.); and the Stanford Dean's Fellowship (to 653 Q.M.). We thank the USTC supercomputing center and the School of Life Science 654 Bioinformatics Center for providing supercomputing resources for this project. H.Y.C. is 655 an Investigator of the Howard Hughes Medical Institute.

656

Disclosure: H.Y.C. is affiliated with Accent Therapeutics (co-founder and advisor), 10X
Genomics (advisor), and Spring Discovery (advisor).

659

660 **REFERENCES**

661

Rinn, J. L. & Chang, H. Y. Genome Regulation by Long Noncoding RNAs. *Annual Review of Biochemistry* 81, 145–166 (2012).

- Fu, X.-D. Non-coding RNA: a new frontier in regulatory biology. *National Science Review* 1, 190–204 (2014).
- Khalil, A. M. *et al.* Many human large intergenic noncoding RNAs associate with
 chromatin-modifying complexes and affect gene expression. *Proceedings of the National Academy of Sciences* 106, 11667–11672 (2009).

669	4.	Flynn, R. A. & Chang, H. Y. Long Noncoding RNAs in Cell-Fate Programming
670		and Reprogramming. Cell Stem Cell 14, 752–761 (2014).
671	5.	Djebali, S. et al. Landscape of transcription in human cells. Nature 489, 101-108
672		(2012).
673	6.	Liu, S. J. et al. CRISPRi-based genome-scale identification of functional long
674		noncoding RNA loci in human cells. Science 355, aah7111 (2017).
675	7.	Sauvageau, M. et al. Multiple knockout mouse models reveal lincRNAs are
676		required for life and brain development. <i>eLife</i> 2 , e01749 (2013).
677	8.	Xu, J. & Cao, X. Long noncoding RNAs in the metabolic control of inflammation
678	0.	and immune disorders. <i>Cellular and Molecular Immunology</i> 16 , 1–5 (2019).
679	9.	Tsai, MC. <i>et al.</i> Long noncoding RNA as modular scaffold of histone
680).	modification complexes. <i>Science</i> 329 , 689–693 (2010).
681	10.	West, J. A. <i>et al.</i> The Long Noncoding RNAs NEAT1 and MALAT1 Bind Active
682	10.	Chromatin Sites. <i>Molecular Cell</i> 55 , 791–802 (2014).
683	11.	Lai, F. <i>et al.</i> Activating RNAs associate with Mediator to enhance chromatin
684	11.	architecture and transcription. <i>Nature</i> 494 , 497–501 (2013).
685	12.	Wang, K. C. <i>et al.</i> A long noncoding RNA maintains active chromatin to
686	12.	coordinate homeotic gene expression. <i>Nature</i> 472 , 120–U158 (2011).
687	13.	Zhao, J. <i>et al.</i> Genome-wide identification of polycomb-associated RNAs by RIP-
688	13.	1 0
689	14	seq. <i>Molecular Cell</i> 40 , 939–953 (2010). Darnell, R. B. HITS-CLIP: panoramic views of protein-RNA regulation in living
	14.	
690	15	cells. Wiley Interdiscip Rev RNA 1, 266–286 (2010).
691	15.	G Hendrickson, D., Kelley, D. R., Tenen, D., Bernstein, B. & Rinn, J. L.
692		Widespread RNA binding by chromatin-associated proteins. <i>Genome Biology</i> 17 ,
693	10	674 (2016).
694	16.	Mondal, T., Rasmussen, M., Pandey, G. K., Isaksson, A. & Kanduri, C.
695		Characterization of the RNA content of chromatin. <i>Genome Research</i> 20 , 899–907
696	17	
697	17.	Bhatt, D. M. <i>et al.</i> Transcript Dynamics of Proinflammatory Genes Revealed by
698	10	Sequence Analysis of Subcellular RNA Fractions. <i>Cell</i> 150 , 279–290 (2012).
699 700	18.	Werner, M. S. & Ruthenburg, A. J. Nuclear Fractionation Reveals Thousands of
700		Chromatin-Tethered Noncoding RNAs Adjacent to Active Genes. <i>Cell Report</i> 12,
701	10	1089–1098 (2015).
702	19.	Li, X. et al. GRID-seq reveals the global RNA-chromatin interactome. Nature
703		<i>Biotechnology</i> 35 , 940–950 (2017).
704	20.	Sridhar, B. et al. Systematic Mapping of RNA-Chromatin Interactions In Vivo.
705		<i>Current Biology</i> 27 , 602–609 (2017).
706	21.	Quinodoz, S. A. et al. Higher-Order Inter-chromosomal Hubs Shape 3D Genome
707		Organization in the Nucleus. Cell 174, 744–757.e24 (2018).
708	22.	Margueron, R. & Reinberg, D. The Polycomb complex PRC2 and its mark in life.
709		<i>Nature</i> 469 , 343–349 (2011).
710	23.	Soibam, B. Super-IncRNAs: identification of IncRNAs that target super-enhancers
711		via RNA:DNA:DNA triplex formation. RNA 23, 1729–1742 (2017).
712	24.	Chu, C., Qu, K., Zhong, F. L., Artandi, S. E. & Chang, H. Y. Genomic maps of
713		long noncoding RNA occupancy reveal principles of RNA-chromatin interactions.
714		Molecular Cell 44, 667–678 (2011).

- Shah, R. N. *et al.* Examining the Roles of H3K4 Methylation States with
 Systematically Characterized Antibodies. *Molecular Cell* 72, 162–177.e7 (2018).
- Simon, M. D. *et al.* High-resolution Xist binding maps reveal two-step spreading during X-chromosome inactivation. *Nature* 504, 465–469 (2013).
- Pandey, R. R. *et al.* Kcnq1ot1 Antisense Noncoding RNA Mediates LineageSpecific Transcriptional Silencing through Chromatin-Level Regulation. *Molecular Cell* 32, 232–246 (2008).
- Monnier, P. *et al.* H19 lncRNA controls gene expression of the Imprinted Gene Network by recruiting MBD1. *Proceedings of the National Academy of Sciences* 110, 20693–20698 (2013).
- Royce-Tolland, M. E. *et al.* The A-repeat links ASF/SF2-dependent Xist RNA
 processing with random choice during X inactivation. *Nature Structural & Molecular Biology* 17, 948–U55 (2010).
- 728 30. Chu, C. *et al.* Systematic Discovery of Xist RNA Binding Proteins. *Cell* 161, 404–
 729 416 (2015).
- Tanscriptome Structure. *Cell* 165, 1267–1279 (2016).
- Ang, C. E. *et al.* The novel lncRNA lnc-NR2F1 is pro-neurogenic and mutated in
 human neurodevelopmental disorders. *eLife* 8, 377 (2019).
- McLean, C. Y. *et al.* GREAT improves functional interpretation of cis-regulatory
 negions. Nature Biotechnology 28, 495–501 (2010).
- 34. Simon, M. D. *et al.* The genomic binding sites of a noncoding RNA. *Proceedings* of the National Academy of Sciences 108, 20497–20502 (2011).
- Time Stephene Stephen
- 74036.Ritchie, M. E. *et al.* limma powers differential expression analyses for RNA-
sequencing and microarray studies. *Nucleic Acids Research* 43, e47–e47 (2015).
- 37. Subramanian, A. *et al.* Gene set enrichment analysis: a knowledge-based approach
 for interpreting genome-wide expression profiles. *Proceedings of the National Academy of Sciences* 102, 15545–15550 (2005).
- Yu, F. *et al.* LnChrom: a resource of experimentally validated lncRNA-chromatin interactions in human and mouse. *Database* 2018, 354 (2018).
- 747 39. Zviran, A. *et al.* Deterministic Somatic Cell Reprogramming Involves Continuous
 748 Transcriptional Changes Governed by Myc and Epigenetic-Driven Modules. *Cell*749 *Stem Cell* 24, 328–341.e9 (2019).
- Rando, O. J. & Chang, H. Y. Genome-Wide Views of Chromatin Structure. *Annual Review of Biochemistry* 78, 245–271 (2009).
- Flynn, R. A. *et al.* 7SK-BAF axis controls pervasive transcription at enhancers. *Nature Structural & Molecular Biology* 23, 231–238 (2016).
- 42. Wang, Z. *et al.* Combinatorial patterns of histone acetylations and methylations in the human genome. *Nature Genetics* **40**, 897–903 (2008).
- 43. Ernst, J. *et al.* Mapping and analysis of chromatin state dynamics in nine human cell types. *Nature* 473, 43–49 (2011).
- 44. Ernst, J. & Kellis, M. ChromHMM: automating chromatin-state discovery and characterization. *Nature Methods* 9, 215–216 (2012).

760	45.	Rousseeuw, P. J. Silhouettes: A graphical aid to the interpretation and validation of
761		cluster analysis. Journal of Computational and Applied Mathematics 20, 53-65
762		(1987).
763	46.	Hirata, H. et al. Long Noncoding RNA MALAT1 Promotes Aggressive Renal Cell
764		Carcinoma through Ezh2 and Interacts with miR-205. Cancer Research 75, 1322-
765		1331 (2015).
766	47.	Jia, J. et al. Long noncoding RNA DANCR promotes invasion of prostate cancer
767		through epigenetically silencing expression of TIMP2/3. Oncotarget 7, 37868-
768		37881 (2016).
769	48.	Quek, X. C. <i>et al.</i> lncRNAdb v2.0: expanding the reference database for functional
770		long noncoding RNAs. <i>Nucleic Acids Research</i> 43 , D168–73 (2015).
771	49.	Wang, X. <i>et al.</i> Molecular analysis of PRC2 recruitment to DNA in chromatin and
772		its inhibition by RNA. <i>Nature Structural & Molecular Biology</i> 24, 1028–1038
773		(2017).
774	50.	Beltran, M. <i>et al.</i> The interaction of PRC2 with RNA or chromatin is mutually
775	50.	antagonistic. Genome Research 26, 896–907 (2016).
776	51.	Meshorer, E. <i>et al.</i> Hyperdynamic plasticity of chromatin proteins in pluripotent
777	51.	embryonic stem cells. <i>Developmental Cell</i> 10 , 105–116 (2006).
778	52.	Bernstein, B. E. <i>et al.</i> A Bivalent Chromatin Structure Marks Key Developmental
779	52.	Genes in Embryonic Stem Cells. <i>Cell</i> 125 , 315–326 (2006).
780	53.	Wapinski, O. L. <i>et al.</i> Hierarchical Mechanisms for Direct Reprogramming of
781	55.	Fibroblasts to Neurons. <i>Cell</i> 155 , 621–635 (2013).
782	54.	Kertesz, M. <i>et al.</i> Genome-wide measurement of RNA secondary structure in
783	54.	yeast. Nature 467, 103–107 (2010).
784	55.	Spitale, R. C. <i>et al.</i> Structural imprints in vivo decode RNA regulatory
785	55.	mechanisms. <i>Nature</i> 519 , 486–490 (2015).
786	56.	Hofacker, I. L. Vienna RNA secondary structure server. <i>Nucleic Acids Research</i>
787	50.	31, 3429–3431 (2003).
788	57.	Wan, Y. <i>et al.</i> Landscape and variation of RNA secondary structure across the
789	57.	human transcriptome. <i>Nature</i> 505 , 706–709 (2014).
790	58.	Sun, D. <i>et al.</i> LncRNA GAS5 inhibits microglial M2 polarization and exacerbates
791	50.	demyelination. <i>EMBO reports</i> 18 , 1801–1816 (2017).
792	59.	Sun, L. <i>et al.</i> RNA structure maps across mammalian cellular compartments.
793	57.	Nature Structural & Molecular Biology 26 , 322–330 (2019).
794	60.	Roost, C. <i>et al.</i> Structure and Thermodynamics of N 6-Methyladenosine in RNA:
795	00.	A Spring-Loaded Base Modification. <i>Journal of the American Chemical Society</i>
796		
790 797	61	137 , 2107–2115 (2015).
	61.	Liu, N. & Pan, T. N6-methyladenosine–encoded epitranscriptomics. <i>Nature</i>
798 700	60	Structural & Molecular Biology 23, 98–102 (2016).
799	62.	Batista, P. J. <i>et al.</i> m6A RNA Modification Controls Cell Fate Transition in Maximum Line Fundamental Stars Cells Cell Stars Cell 15 , 707, 710 (2014)
800		Mammalian Embryonic Stem Cells. Cell Stem Cell 15, 707–719 (2014).
801		
802		
803		
804		
805		

806 FIGURE LEGENDS

807

808 Figure 1. PIRCh-seq enables effective chromatin-RNA association *in vivo*

- 809 A. Schematic representation of PIRCh approach followed by high-throughput sequencing.
- **B.** Normalized input and histone H3 PIRCh-seq profiles of lncRNA *XIST* in human female fibroblasts.
- 812 **C.** PIRCh-qPCR analysis in mouse neuronal stem cells (NSCs, orange) and adult brain 813 (purple) shows that *Xist* is attached to chromatin H3 compared with Actin control.
- 814 **D-E.** Normalized input and PIRCh-seq profiles with histone modifications of H3K4me3,
- 815 H3K27ac, and H3K27me3 at the lncRNA *Xist* (**D**) and *lnc-Nr2f1* (**E**) locus in mouse 816 neuronal precursor cells (NPC).
- 817 F. Normalized input and ChIRP-seq profiles of lncRNA lnc-Nr2f1 in NPC, and
- 818 H3K4me3, H3K27ac, H3K4me1 and H3K27me3 ChIP-seq profiles in NPC. Showing 819 *Clcn4* gene locus as an example.
- G. Average coverage of ChIP-seq signal (Reads per million over Input) around (+/-10kb)
 lnc-Nr2f1 ChIRP-seq peaks in NPC.
- 822

Figure 2. ncRNAs are enriched on chromatin compare with protein coding
transcripts

A. Ratio of intronic over exonic reads obtained from different chromatin-RNA
association sequencing technologies (GRID, CPE, CAR, and PIRCh) versus input
controls in multiple cell lines.

B. Normalized average read coverage around introns from different chromatin-RNA association sequencing technologies (GRID, CPE, CAR, and PIRCh) versus input controls in multiple cell lines.

831 C. Normalized average read coverage around introns from histone modification specific

- 832 PIRCh-seq profiles (colored) and inputs (black) in mouse embryonic stem cells (mESCs).
- **B D**. Gene set enrichment analysis (GSEA) shows highly statistical enriched (FDR=0,
- P<0.0001) of non-coding genes (Green) and depleted of coding genes (Blue) on histone
 H3 in mESCs. Genes were ranked by their histone H3 PIRCh enrichment scores.

E. Average fold enrichment (calculated by limma in R) of the coding gene, lncRNA, premiRNA, snoRNA and other ncRNA from histone modification specific PIRCh-seq profiles (namely H3, H3K4me1, H3K4me3, H3K27ac, H3K27me3, H3K9me3, and H4K16ac) in mESC. Error bar shows the standard deviation from the mean.

- F. Average variation score of the PIRCh-seq signals for the coding versus non-coding
 genes (****P<0.0001, two-tailed Welch's T-test). Error bar shows the standard deviation
 from the mean.
- 843 G. Heatmap displaying the ranking of the ChIP-seq enrichment of the chromatin binding
- sites of 23 lncRNA. The 23 lncRNAs are chromatin enriched from PIRCh-seq and the
- chromatin binding sites are obtained from ChIRP/CHART/RAP/GRID-seq profiles from
- the LnChrom database. Colors represent ranking from 1-5.
- 847 H. Heatmap shows the ranking of PIRCh-seq enrichment of the same lncRNAs in G.848 Colors represent ranking from 1-5.

Fang et al. (CHANG), p.22

- 849 I. Bar plot of the Spearman correlation coefficients between the ranking in G and H for
- each lncRNA versus random permutation (****P<0.0001, two-tailed Welch's T-test).
- 851 J. Unsupervised clustering of the Pearson correlation coefficients matrix of the histone
- modification specific PIRCh-seq profiles based on the enrichment scores from the 258chromatin associated ncRNAs in mESC.
- 854

855 Figure 3. PIRCh-seq classifies functional ncRNAs via chromatin state association

- A. Summary of histone modifications representing distinct regulatory patterns.
- 857 **B.** The enrichment of the *7sk* ChIRP-seq peaks overlap with different histone 858 modification ChIP-seq peaks in the same cell line (mESC). A positive value indicates the 859 ChIRP-seq peaks are highly enriched with ChIP-seq peaks compare to random, and a 860 negative value indicates depletion.
- 861 **C.** The PIRCh enrichment score of the lncRNA *7sk* in mESC from distinct histone 862 modification specific PIRCh-seq experiments. A positive value means enriched, and a 863 negative value means depleted.
- **D.** Classification of the PIRCh-seq identified chromatin associated ncRNAs (n=258) in mESC. Scatter plot shows the t-SNE result on PIRCh-seq enrichment score matrix and annotated by K-means clustering.
- 867 E. Functional classification of histone specific chromatin-RNA association patterns
 868 defined by chromHMM algorithm.
- 869 **F.** Box plot of the expression of the coding genes nearby (+/-100Kb) each group of
- PIRCh clustered ncRNAs defined in **D**. Center lines represent mean values; box limits represent the interquartile range; whiskers each extend 1.5 times the interquartile range; dots represent outliers. The expression of the coding genes that close to the ncRNAs in the "repressed" group is significantly lower than those in the "active promoter/enhancer" group (P<0.05, two-tailed Welch's T-test). Genes close to un-enriched ncRNAs are shown as control.
- 876

877 Figure 4. Cell type specific chromatin association of ncRNAs

- A. Number of chromatin enriched RNAs in mESC, MEF and NPC.
- **B**. Unsupervised clustering of the Pearson correlation coefficients matrix of the histone modification specific PIRCh-seq profiles in mESC, MEF and NPC, based on the enrichment scores from the 458 chromatin associated ncRNAs in each cell type.
- 882 C. Ratio of the chromatin enriched ncRNA under each chemical modification over the883 total number of enriched ncRNAs in mESC, MEF, and NPC.
- 884 **D.** Schematic illustration of how RNAs enriched on both the repressive and active 885 chromatin (bi-chromatin enriched) and either the repressive or active chromatin (mono-886 chromatin enriched).
- 887 E. UCSC tracks of the normalized PIRCh-seq signal at the lncRNA uc008bcq.1 locus in
- 888 mESC, MEF and NPC. *uc008bcq.1* is bi-chromatin enriched in mESC, but monochromatin enriched in MEF and NPC.
- **F.** Number of ncRNAs that are bi-chromatin enriched or mono-chromatin enriched in mESC, MEF and NPC (***P<0.001, *P<0.05, Chi-square test).

892

Figure 5. RNA with single strand are more likely to associate with chromatin.

A. UCSC track of the normalized input (black) and H3 (red) and H3K4me3 (green)
PIRCh-seq signals of lncRNA *Malat1* in mESC. Bottom peaks are chromatin enriched
sites on *Malat1*.

897 B. Structure profile from icSHAPE and structural prediction from RNAfold around a898 zoom in chromatin associated peak on lncRNA *Malat1*.

- C. Computational workflow to integrate RNA secondary structure information from
 icSHAPE and chromatin enrichment information from PIRCh-seq to study the structural
 preference of chromatin-RNA association.
- 902 D. Average diagram of icSHAPE scores around all PIRCh-seq peaks under different
 903 histone modifications (colored solid line) versus a randomly selected background (grey
 904 solid line). P-values (colored dash line) were estimated by using two-tailed Welch's T905 test on every position between PIRCh-seq profiles over background.
- 906 E. Box-plot of the icSHAPE score of PIRCh-seq enriched vs depleted RNAs
 907 (***P<0.001, two-tailed Welch's T-test). Center lines represent mean values; box limits
 908 represent the interquartile range; whiskers each extend 1.5 times the interquartile range;
 909 dots represent outliers.
- 910 F. Box-plot of the PIRCh-seq enrichment scores of the top 100 most single stranded
 911 RNAs versus the top 100 most double stranded RNAs based on icSHAPE scores
 912 (**P<0.01 two-tailed Welch's T-test). Center lines represent mean values; box limits
 913 represent the interquartile range; whiskers each extend 1.5 times the interquartile range;
 914 dots represent outliers.
- 915 G. Relative allele specific RNA expression and chromatin enrichment of lncRNAs Xist,
- Gas5 and Malat1 in the 129S1 allele versus the CAST allele of NPC. The 129S1 version
- 917 of lncRNA *Xist* is highly expressed and also enriched at chromatin with H3K27me3 918 modification. Both alleles of lncRNA *Malat1* were almost equally expressed and 919 enriched. The 129S1 version of *Gas5* was lowly expressed but highly enriched on 920 chromatin compared to the CAST version of the same gene.
- 921 **H.** Normalized allele specific input and histone H3K27me3 PIRCh-seq signals in the
- 922 129S1 and CAST alleles. Top shows single nucleotide polymorphisms (SNP) positions
- 923 that distinguish the alleles.
- 924

Supplementary Figure 1. Quality control of histone modification specific PIRCh-seq experiments on distinct cell types.

- 927 A-C. The specificity of IP of different antibodies H3K4me1 (A), H3K4me3 (B), and
- 928 H3K27me3 (C) after glutaraldehyde crosslinking using modified mononucleosomes with 929 barcodes. 7 different mononucleosomes with barcodes were tested.
- 930 **D.** Table summarizing PIRCh-seq experiments performed in this paper.
- 931 E. Kernel density estimation (KDE) plot of the gene expression from different subcellular
- 932 RNA sequencing data and PIRCh-seq data.

Fang et al. (CHANG), p.24

F-M. Scatter plots of expressed transcripts (log2) in two PIRCh-seq replicates with
 correlation score R on different histone modification, H3, H3K4me1, H3K4me3,

- 935 H3K27ac, H3K27me3, H3K9me3, and H4K16ac respectively.
- 936

937 Supplementary Figure 2. PIRCh-seq effectively and finely enriches RNA associated 938 with chromatin

- A-B. Normalized UCSC tracks of input and histone H3 PIRCh-seq signals on lncRNA *KCNQ10T1*(A) in human female fibroblast cells and *H19* (B) in human H9 embryonic
 stem cells.
- 942 **C-D.** Normalized UCSC tracks of input and histone H3 PIRCh-seq signals on protein 943 coding genes *ACTB* (**C**), and *EEF2* (**D**) in human female fibroblast cells.
- 944 E-F. Normalized UCSC tracks of input and histone modification specific PIRCh-seq
- signals on protein coding gene Actb (\mathbf{E}) and Eef2 (\mathbf{F}) in mouse neuronal precursor cells.
- 946 G. Top 5 enriched gene ontology of the *lnc-Nr2f1* ChIRP-seq peaks using GREAT.
- 947

948 Supplementary Figure 3. PIRCh-seq captures low nascent transcription

- 949 A-E. Scatter plot of the PIRCh-seq (y-axis) signal over input vs the corresponding ChIP-
- 950 seq (x-axis) signal over input for all the expressed genes in mESC, with linear regression
- 951 (red dotted line). Colors represent the density of point.
- 952

953 Supplementary Figure 4. ncRNAs are more enriched on chromatin than protein954 coding genes.

- A-B. Box-plots of the PIRCh-seq signal before (A) and after (B) normalization using the
 limma algorithm in R. cpm represents count per million, and log scale is shown. Center
 lines represent mean values; box limits represent the interquartile range; whiskers each
 extend 1.5 times the interquartile range; dots represent outliers.
- 959 C. Circle plots showing the distribution of the expressed (inner circle) and PIRCh
 960 enriched (outer circle) RNA types associated with different histone modifications.
 961 ncRNAs are highly enriched in PIRCh compared with coding genes.
- 962 D. Total length of the genomic regions (in bp) covered by each histone modification963 ChIP-seq peak in mESC.
- 964

Supplementary Figure 5. The chromatin-RNA association of ncRNAs give a hint of *cis* regulation.

- A. Bar chart showing the number of ncRNAs enriched at chromatin with specific histonemodifications in mESC.
- 969 **B.** The odds ratio of the PIRCh enriched ncRNAs overlap with the chromatin enriched
- 970 ncRNAs defined in lncRNAdb. "Yes" means the ncRNA is both PIRCh enriched and
 971 found in lncRNAdb, and "No" means PIRCh enriched but was not identified in
 972 lncRNAdb.
- 973 **C.** Box-plot of the expression of the coding genes near (+/-100Kb) each group of histone
- 974 modification specific PIRCh-seq enriched ncRNAs. Center lines represent mean values;
- 975 box limits represent the interquartile range; whiskers each extend 1.5 times the

Fang et al. (CHANG), p.25

976 interquartile range; dots represent outliers. The expression of the coding genes that close

- to the ncRNAs enriched on active chromatin shows no significant difference between that
- 978 with repressed chromatin.
- 979 D. Box-plot of the expression of each groups of PIRCh cluttered ncRNAs defined in
- 980 Figure 3D. Center lines represent mean values; box limits represent the interquartile
- range; whiskers each extend 1.5 times the interquartile range; dots represent outliers.
- 982

Supplementary Figure 6. Pattern of ncRNA chromatin association is generally conserved in distinct cell types.

- A. Normalized average read coverage around introns from histone modification specific
 PIRCh-seq profiles (colored) and inputs (black) in MEF.
- 987 B. Gene set enrichment analysis (GSEA) shows highly statistical enriched (FDR=0,
- 988 P<0.0001) of non-coding genes (Green) and depleted of coding genes (Blue) on histone
- H3 in MEF. Genes were ranked by their histone H3 PIRCh enrichment scores.
- C. Average fold enrichment (calculated by limma in R) of the coding gene, lncRNA, premiRNA, snoRNA and other ncRNA from histone modification specific PIRCh-seq
 profiles (namely H3, H3K4me1, H3K4me3, H3K27ac, H3K27me3, H3K9me3, and
 H4K16ac) in MEF. Error bar shows the standard deviation from the mean.
- 994 **D.** Functional classification of histone specific chromatin-RNA association patterns995 defined by chromHMM algorithm.
- 996 E. Classification of the PIRCh-seq identified chromatin associated ncRNAs (n=200) in
- MEF. Scatter plot shows the t-SNE result on PIRCh-seq enrichment score matrix andannotated by K-means clustering.
- 999 **F.** Normalized input, Igg and H3 PIRCh-seq profiles of lncRNA *Pvt1* in MEF.
- 1000

Supplementary Figure 7. Allele specific RNA secondary structure and chromatin enrichment of lncRNA Gas5.

- 1003 **A-B.** RNAfold predicted the secondary structure of the 129S1 (**A**) and CAST (**B**) allele 1004 of *Gas5*. RiboSNithes are noted in blue and bases attached to chromatin (peaks) are 1005 shown in red.
- 1006 C. Structural information of 129S1 allele around the PIRCh enriched peak region. Data1007 obtained from icSHAPE experiments on mESC.
- 1008

1009 Supplementary Figure 8. RNA m⁶A methylation affects chromatin-RNA association.

- A. Distribution of histone H3 and other chemical modification PIRCh-seq peaks alongscaled transcripts.
- 1012 **B-C.** Average diagrams of m^6A modification scores around bases attached to chromatin 1013 (peaks) from histone H3 (**B**) and all chemical modification specific (**C**) PIRCh-seq 1014 profiles, versus that from randomly selected background.
- 1015

1016 Supplementary Table 1 Chromatin enriched ncRNAs in all mouse samples.

- 1017 Supplementary Table 2 Allele specific chromatin enrichment in NPC.
- 1018

1019 **METHODS**

1020

1021 Cell culture

1022 V6.5 mouse ES cells were cultured on 0.2% gelatin-coated plates at 37°C with mES 1023 media: 500ml Knockout DMEM (Gibco), 90ml FBS, 6ml non-essential amino acid 1024 (NEAA, 100x, Gibco), 6ml glutamine or glutamax (200mM stock solution), 6ml 1025 Pen/Strep, 1ml BME and 60µlLIF (Millipore, ESG1106). Mouse embryonic fibroblast 1026 (MEF) cells were cultured at 37 °C and 5% CO2 in: 450ml DMEM, 50ml FBS, 5ml 1027 Pen/Strep, 5ml NEAA, 5ml pyruvate, 4ul beta-Mercaptoethanol. Mouse Neural Precursor 1028 cells (NPCs) were cultured in N2B27 medium (DMEM/F12 (Invitrogen, 11320-033), Neurobasal (Gibco, 21103-049), NDiff Neuro-2 Medium Supplement (Millipore, 1029 1030 SCM012), B27 Supplement (Gibco, 17504-044)) supplemented with EGF and FGF (10 1031 ng/ml, each) (315-09 and 100-18B, Peprotech). Cells were passaged using Accutase 1032 (SCR005, Millipore) and cultured on 0.2% gelatin-coated plates. H9 human embryonic 1033 stem cells were seeded in a feeder-free system using Matrigel hESC-Qualified Matrix (354277, Corning) and were maintained in Essential 8 media (A1517001, Thermo Fisher 1034 Scientific) as described previously¹. Cells were passaged every three days as clumps with 1035 0.5mM EDTA¹. Human Female Fibroblasts (HFF) were cultured at 37 °C and 5% CO2 in 1036 1037 DMEM supplemented with 1% pen/strep and 10% FBS.

1038 **PIRCh-seq library preparation**

To harvest the cells for PIRCh-seq, approximately 4×10^7 cells were trypsinized and 1039 1040 pooled into a 50ml falcon tube, after washing with 40ml of cold PBS once. Fresh 1% 1041 glutaraldehyde in room temperature PBS was created from 25% stock and remaining 1042 stock was discarded. The cell pellet was resuspended in 1ml of glutaraldehyde solution 1043 and a p1000 pipette was used to resuspend cells, and to top up to 40ml (1ml 1% 1044 glutaraldehyde / 1 million cells). After inverting several times, the tube was gently 1045 shaken for 10 minutes, and then quenched with 1/10 volume of 1.25M glycine. The tube 1046 was inverted several times, shaken gently for 5 min, and spun down 2000g for 4 min. The 1047 pellet was then washed once with 40ml cold PBS. The pellet was responded in 1ml/20million cells of cold PBS. Cells were aliquoted at 1ml each to a fresh eppendorf 1048 1049 tube, and spun down 2000g for 4 min. After, supernatant was carefully aspirated, cell 1050 pellets were flash frozen, and stored at -80°C if necessary.

1051

For sonication, prepared cell pellets were spun down at 2000g for 4 min and any remaining PBS was removed. Lysis per 20 million cells was performed with 1ml of lysis buffer (1% SDS, 50mM Tris 7.0, 10mM EDTA, 1mM PMSF, 0.1U/ul Superase-in (Ambion), 1x Proteinase inhibitor (Roche)). Lysate was then sonicated till the chromatin size was ~300-2000bp and the lysate was clear. The lysates were spun down at 16000g for 10 min. Supernatants were flash frozen and stored at -80°C if necessary.

1058

1059 For PIRCh-seq library construction, chromatin was thawed and 10ul was taken as input. 1060 200ul were aliquoted per reaction, and 400ul dilution buffer was added to each reaction. 1061 H3 or a specific histone modification antibody was then added (Dilution buffer: 0.01% 1062 SDS, 1.1% Triton X 100, 1.2 mM EDTA, 16.7 mM Tris 7.0, 167 mM NaCl, 1mM PMSF, 1063 0.1U/ul Superase-in (Ambion), 1x Proteinase inhibitor (Roche)). The reaction was shaken end-to-end at 4°C overnight. 50ul Protein A dynabeads was used per 5ug antibody IP. 1064 1065 Beads were washed with 5 times the original volume of dilution buffer 4 times. Notice 1066 that it is important not to exceed 200ul original volume of beads per tube. During the last wash, beads were aliquoted to 1 tube per reaction. The buffer was aspirated and, 200ul of 1067 1068 the IP sample was used to resuspend and transfer beads to the IP sample. The reaction 1069 was shaken end-to-end at room temperature for 2 hours. The beads were then washed 1070 with 1ml wash buffer 4 times, and resuspended in 50ul IP elution buffer (1% SDS, 50mM 1071 NaHCO3). The reaction was then vortexed at setting 1 for 15 min. The supernatant was 1072 then transferred to a fresh tube and the bead elution was repeated. The supernatant was 1073 combined for a total of 100ul. 5ul 3M NaOAc was immediately added to neutralize pH. 1074 10ul TurboDnase buffer and 1ul TurboDnase (Ambion) were added and the reaction was 1075 incubated 37°C for 30min. 3ul 500mM EDTA was added to eliminate divalent ions. 5ul 1076 Proteinase K (Ambion) was added, and the reaction was incubated at 50°C for 45 min.

1077

1078 To make our sequencing libraries, we extracted RNA using Trizol/chloroform, and precipitated the RNA with an equal volume of isopropanol. RNA pellet was washed in 1079 1080 1ml 70% EtOH, and pellets were resuspended in 10ul H2O. 1ul TurboDnase buffer was 1081 added, followed by 1ul TurboDnase, and the reaction at 37°C for 30min. 1.2ul of 1082 TurboDnase inactivating reagents were added. The reaction was vortexed for 3 minutes 1083 and spun down. The 10ul supernatant was heated at 75°C for 10 minutes to kill DNase. 1084 The reaction was purified using a Nugen Ovation v2 kit and eluted in 5uL for library 1085 preparation.

1086

1087 ChIRP-seq library preparation

To determine the genome-wide localization of *lnc-Nr2f1* we followed protocols 1088 previously described². ChIRP was performed using biotinylated probes designed against 1089 mouse lnc-Nr2f1 using the ChIRP probes designer (Biosearch Technologies). 1090 Independent even and odd probe pools were used to ensure lncRNA-specific retrieval as 1091 protocols previously described³. "Even" and "odd" sets of probes shared no overlapping 1092 1093 sequences, as we performed two independent ChIRP-seq experiments with these two sets 1094 of probes separately. Two sets of data were then combined for downstream analysis (see 1095 below). Mouse NPC samples are crosslinked in 3% formaldehyde. RNase pre-treated 1096 samples are served as negative controls for probe-DNA hybridization. ChIRP libraries are 1097 constructed using the NEBNext DNA library preparation kit (New England Biolabs).

Sequencing libraries were barcoded using TruSeq adapters and sequenced on HiSeq orNextSeq instruments (Illumina).

1100

1101 Experimental validation of antibody specificity after glutaraldehyde crosslinking 1102 using modified mononucleosomes with barcodes

1103 To ensure that chemical crosslinking with glutaraldehyde did not affect antibody 1104 specificity, we followed previous study to test antibody specificity using SNAP-ChIP⁴. 1105 During IP pulldown, 15 uL of recombinant nucleosomes (SNAP-ChIP, EpiCypher, 19-1106 1001) were fixed with fresh 1% glutaraldehyde. 1% glutaraldehyde was prepared on the 1107 same day in room temperature PBS from 25% stock. Fixation was performed for 10 1108 minutes at room temperature with gentle shaking. The reaction was then quenched with 1109 1/10 of the original reaction volume of 2.5 M glycine. Tubes were then inverted several 1110 times and incubated for 5 minutes at room temperature with gentle shaking.

1111

1112 500 uL of fixed chromatin were then added to each tube and pipetted up and down 1113 several times to mix well. 10 uL of nucleosomes mixed with chromatin were taken out of 1114 each tube to be used as input during the qPCR. One tablet of Roche cOmplete protease 1115 inhibitor was dissolved (Roche, 11697498001) in 50 mL of DI water to obtain a working 1116 solution of 50x protease inhibitor cocktail. 60 uL of 50x protease inhibitor was added to 1117 3mL of blank dilution buffer (0.01% SDS, 1.1% Triton X100, 1.2 mM EDTA, 16.7 mM 1118 Tris pH 7.0, 167 mM NaCl). 1 mL of dilution buffer with protease inhibitor was then 1119 added to each reaction. 5 ug of appropriate detection antibody for IP pulldown was added 1120 to 300 uL of chromatin mixed with crosslinked nucleosomes for each condition. Samples 1121 were then incubated at 4°C overnight with end-to-end shaking.

1122

IP product was eluted as specified during PIRCH library construction. DNA of interest was purified using a Zymo DNA Clean and Concentrator-5 kit (Zymo Research, D4013). The qPCR reaction was performed using Roche's LightCycler and Brilliant II SYBR® Green QRT-PCR Master Mix (Agilent). We analyzed enrichment for target histone modifications by amplifying unique DNA barcodes at the 3' end, using primer sequences provided by EpiCypher.

1129

1130 **RT-qPCR**

1131 For qRT-PCR analysis, we used Roche's LightCycler and Brilliant II SYBR® Green1132 QRT-PCR Master Mix (Agilent).

1133

1134 **PIRCh-seq data alignment**

1135 Raw reads were uniquely mapped to mm9/hg19 using Tophat with default parameters⁵.

1136 Samtools and BedTools were used to transform the mapped bam file into bedGraph and

- 1137 bigwig files for visualization on the UCSC genome browser^{6,7}. RPKM and raw reads
- 1138 count for each gene were calculated by self-designed scripts with ensemble annotation,

1139 Homo_sapiens.GRCh37.75.gtf for human and Mus_musculus.NCBIM37.67.gtf, and a 1140 number of previous publications for mouse samples respectively⁸.

1141

1142 Calculate exon/intron ratio to estimate nascent transcripts

1143 To compare the exon/intron ratios between the PIRCh-seq profiles and other chromatin 1144 associated RNA detection technologies, we aligned raw reads to the same hg19 genome 1145 index with Tophat and calculated the reads mapped to intron/exon with ensemble annotation gtf file as described above⁵. For the average read counts around introns, three 1146 steps were taken: (1) scaled every intron based on its length, and extended 1 intron length 1147 1148 up and down stream of the selected intron; (2) divided the entire region to 300 windows, 1149 and calculate the average number of read counts mapped in each window and then take log2 to scale down the values to avoid interferences from the outliers; (3) take average 1150 1151 for all the windows among all introns. To estimate the correlation between the histone 1152 modification-specific PIRCh-seq profile with its corresponding ChIP-seq signals, we 1153 obtained ChIP-seq profiles of each histone modification in mESC from ENCODE. And 1154 then, for each expressed gene in mESC, the histone modification ChIP-seq signal over 1155 input on the gene exon were calculated as the ChIP signal for that gene, and were 1156 compared with the corresponding PRICh-seq enrichment score with the same histone 1157 modification, and our results indicated that there was no significant correlation with these 1158 two sets of signals.

1159

1160 Gene set enrichment analysis (GSEA)

1161 GSEA software was downloaded from (http://software.broadinstitute.org/gsea/index.jsp) 1162 at the Broad Institute website and was utilized to perform the significant differential 1163 chromatin enrichment from PIRCh-seq against ncRNA versus coding genes⁹. The 1164 ncRNA set was consist of the annotated snoRNA, snRNA, rRNA, lncRNA, miRNA and 1165 miscRNA.

1166

1167 Data normalization and identification of the chromatin enriched RNAs

The chromatin enriched ncRNAs were identified through the limma algorism in R¹⁰. First, 1168 1169 a data matrix was obtained, where each raw read was a gene and each column a sample, 1170 and the element of the matrix represented the number of raw reads from PIRCh-seq 1171 experiments and inputs. The values in this matrix were then normalized by the limma-1172 voom method in R. After that, differential analysis was performed using the limma gene-1173 wise linear model for each pair of PIRCh replicates over inputs. Non-coding RNAs with 1174 P-value<0.05 and log2 fold change over inputs>0 were defined as chromatin enriched. 1175 We obtained 258 chromatin enriched ncRNAs in mouse V6.5 cell line, 200 in MEF and 1176 110 in NPC. Variation score of each gene was defined as the standard deviations of the 1177 fold change among all histone modification specific PIRCh-seq profiles. The Pearson

1178 correlation coefficients between each two PIRCh-seq experiments were calculated and 1179 unsupervised clustering of the correlation matrix was performed in Cluster.

1180

1181 Computational validation of the PIRCh-seq enriched ncRNAs.

In order to validate the PIRCh-enriched candidates by similar methods, we examined 96 1182 1183 chromatin-association datasets from ChIRP/CHART/RAP/GRID-seq published experiments collected by the LnChrom database¹¹. We found a total of 23 expressed 1184 lncRNAs in the LnChrom database, including Xist, Firre, Rmrp, Tug1 and etc., and all of 1185 1186 them were positively enriched in our PIRCh experiment and 14 of which were significant 1187 with P-value<0.05, suggesting the high sensitivity of the PIRCh approach in identifying 1188 chromatin associated lncRNAs. Furthermore, we obtained the genomic binding sites 1189 (peaks) of 23 lncRNAs from the aforementioned experiments, and overlapped them with the histone ChIP-seq peaks¹² and got a ratio of the overlap for each lncRNA. We then 1190 calculated the Spearman correlation coefficients of these ratios with their corresponding 1191 lncRNA's PIRCh-seq enrichment scores in the same cell line (normalized by the total 1192 1193 number of different ChIP-seq peaks), and found that these correlations were significantly higher than random permutations. Peak calling was performed by MACS2¹³ with 1194 FDR<0.05. 1195

1196

1197 The chromatin association states of the enriched ncRNAs

1198 To cluster chromatin-enriched ncRNAs in distinct groups for functional prediction, we 1199 performed t-SNE and K-mean clustering on the PIRCh enrichment score matrix with the 1200 chromatin associated ncRNAs. The proper K number (K=6) was determined by silhouette 1201 score¹⁴.

1202

1203 Nearby coding gene expression comparison.

To further evaluate the functional prediction for chromatin enriched ncRNAs, we first grouped chromatin enriched ncRNAs by functional classification, and then obtained lists of the nearby (+/-100Kb) coding genes. We then calculated the gene expressions of these coding genes and represented them in box-plots. Similarly, we obtained a different list of nearby coding genes if the chromatin enriched ncRNAs were classified based on their chromatin enrichment scores on each histone modification. The significance between each group was estimated by 2-tail Welch's T-test.

1211

1212 Inc-Nr2f1 ChIPR-seq analysis

1213 To further validate the PIRCh-seq candidates, we performed ChIRP-seq on one of the

1214 H3K4me3 modified PIRCh-seq enriched lncRNAs named *lnc-Nr2f1*. Experimental

1215 methods were mentioned above, where independent "even" and "odd" probe sets were

1216 applied. LncRNA *lnc-Nr2f1* ChIRP-seq data were then analyzed by applying a previously

1217 published pipeline³, where the read alignment was performed in bowtie2 and peak calling

Fang et al. (CHANG), p.31

in MACS2. Signals from even and odd ChIRP-seq profiles were then merged to reduce
false positive caused by probes. We confirmed that *lnc-Nr2f1* associated genomic regions
were indeed enriched with H3K4me3 but no other modifications in NPCs, where the
NPC ChIP-seq data was obtained from GSE117289, indicating the high specificity of our
PIRCh-seq approach.

1222

1224 Allelic specific enrichment analysis in NPC

1225 We first built the CAST/EiJ and 129S1/SvImJ reference genome. The vcf files containing 1226 the SNPs in the CAST and 129S1 strains were downloaded from the dbSNP database with the mm9 assembly¹⁵. Their corresponding genome fasta file was made by GATK 1227 toolkit FastaAlternateReferenceMaker and SelectVariants tools¹⁶. After that, the inputs 1228 1229 and PIRCh-seq data in were re-aligned against the CAST and 129S1 indexes by TopHat2 with 0 mismatch (parameter -N 0) to improve the specificity⁵. The allele specific 1230 1231 alignment files were then converted to the bedGraph and bigWigs format using BEDtools. 1232 For each gene, its allele specific expression and enrichment analysis was performed for 1233 every SNP on the list, and estimated the significance between CAST and 129S1 through 1234 the Mann-Whitney-Wilcoxon test, and P-value<0.05 was defined as significant.

1235

1236 Enriched peak calling from PIRCh-seq profiles

1237 To further investigate the underlying mechanism of RNA-chromatin association, we 1238 performed peak calling on PIRCh-seq profiles to identify the bases on each enriched 1239 RNA that were mostly affiliated with histone proteins. We first merged data from two 1240 replicates of each gene to minimize the experimental deviation bias, and smoothed the 1241 normalized read counts on each base through a 5bp sliding window, along with a 2bp step 1242 size. Peak calling was performed on the smoothed signal with a home-made script. We 1243 defined a peak in the local maximum that is 5-fold or more amplified relative to the 1244 median read counts of the transcript. Next, we applied a bootstrap method by randomly 1245 sampling 1000 times with reads from the transcripts, and then estimated the P-value of 1246 each peak as the percentage of cases that were more enriched than observed. Finally, we 1247 calculated the relative fold-change of each peak with respect to the input control. 1248 Significant peaks were filtered based on fold change and P-value. Finally, RNA structural 1249 and modification information was integrated with PIRCh-seq peaks for downstream 1250 analysis.

1251

1252 icSHAPE analysis and structural prediction using RNAfold

To estimate the structure information around PIRCh peak, we integrate mouse V6.5 icSHAPE data from previous paper^{17,18}. Each transcript's icSHAPE score was calculated by the original icSHAPE pipeline with default parameter. We used home-made script to count icSHAPE score around PIRCh peak(+/-200bp) among all transcripts, and the significance between histone-modification PIRCh peak and random background region

Fang et al. (CHANG), p.32

1258 was estimated by by 2-tail Welch's T-test. In terms of Gas5 in NPC, the structure 1259 information of 129S1 allele was represented by V6.5 icSHAPE data, since they have the same sequence. Structure prediction of 129S1 allele and CAST allele was performed by 1260 RNAfold web server with default parameter¹⁹. For 129S1 allele, the higher icSHAPE 1261 score at peak region indicate single strand structure, which is similar to the structure 1262 1263 prediction from RNAfold. Furthermore, structure prediction of CAST allele of Gas5 in 1264 NPC shows that riboSnitches around PIRCh peak might be the cause of the allele specific 1265 enrichment of Gas5's in NPC.

1266

1267 Statistics

For data presented in **Figure 1B** (RT-PCR), P-values were calculated via the Mann-Whitney-Wilcoxon test in Python. For data presented in **Figure 2D & S6B** (GSEA), enrichment score, P-values and FDR were calculated in GSEA. For data presented in **Figure S2G**, binomial P-values were calculated by GREAT. For all T-test presented in this paper, included **Figure 2E, F, I, Figure 3F, Figure S5C, Figure 5D, E, F, G**, Pvalues were calculated via two-tailed Welch's T-test in Python. For data presented in **Figure 4F**, P-values were calculated via the Chi-square Test.

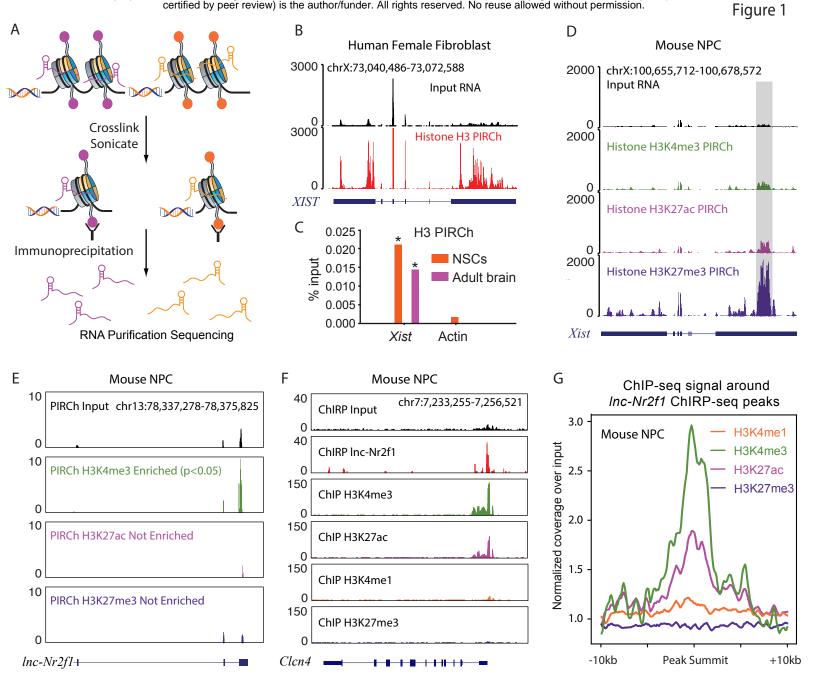
1275

1276 **Data integration**

Mouse v6.5 ChIP-seq results were downloaded from GSE102518¹². Mouse NPC ChIPseq data were downloaded from GSE117289. Mouse 7SK ChIRP-seq results were downloaded from GSE69143²⁰. Murine structural information and RNA modification information were collected from our previous publications^{18,21}. All RNA binding peaks in ChIRP/CHART/RAP/GRID-seq experiments were downloaded from LnChrom¹¹. All mouse data was analyzed using the mm9 assembly and all human data using hg19 assembly.

- 1284 1285 **Reference:**
- 1286
- 1287 1. Chen, G. *et al.* Chemically defined conditions for human iPSC derivation and culture. *Nature Methods* **8**, 424–429 (2011).
- 1289 2. Ang, C. E. *et al.* The novel lncRNA lnc-NR2F1 is pro-neurogenic and mutated in human neurodevelopmental disorders. *eLife* 8, 377 (2019).
- 1291 3. Chu, C., Qu, K., Zhong, F. L., Artandi, S. E. & Chang, H. Y. Genomic maps of long noncoding RNA occupancy reveal principles of RNA-chromatin interactions. *Molecular Cell* 44, 667–678 (2011).
- Shah, R. N. *et al.* Examining the Roles of H3K4 Methylation States with
 Systematically Characterized Antibodies. *Molecular Cell* 72, 162–177.e7 (2018).
- 12965.Trapnell, C. *et al.* Differential gene and transcript expression analysis of RNA-seq1297experiments with TopHat and Cufflinks. *Nature Protocols* 7, 562–578 (2012).
- 1298 6. Li, H. *et al.* The Sequence Alignment/Map format and SAMtools. *Bioinformatics*1299 25, 2078–2079 (2009).

- 1300 7. Quinlan, A. R. & Hall, I. M. BEDTools: a flexible suite of utilities for comparing genomic features. *Bioinformatics* 26, 841–842 (2010).
- 1302 8. Guttman, M. *et al.* Ab initio reconstruction of cell type–specific transcriptomes in
 1303 mouse reveals the conserved multi-exonic structure of lincRNAs. *Nature*1304 *Biotechnology* 28, 503–510 (2010).
- 1305 9. Subramanian, A. *et al.* Gene set enrichment analysis: a knowledge-based approach
 1306 for interpreting genome-wide expression profiles. *Proceedings of the National*1307 *Academy of Sciences* 102, 15545–15550 (2005).
- 1308 10. Ritchie, M. E. *et al.* limma powers differential expression analyses for RNA-1309 sequencing and microarray studies. *Nucleic Acids Research* **43**, e47–e47 (2015).
- 1310
 11. Yu, F. *et al.* LnChrom: a resource of experimentally validated lncRNA-chromatin interactions in human and mouse. *Database* 2018, 354 (2018).
- 1312 12. Zviran, A. *et al.* Deterministic Somatic Cell Reprogramming Involves Continuous
 1313 Transcriptional Changes Governed by Myc and Epigenetic-Driven Modules. *Cell*1314 *Stem Cell* 24, 328–341.e9 (2019).
- 1315 13. Zhang, Y. *et al.* Model-based analysis of ChIP-Seq (MACS). *Genome Biology* 9, 1316
 R137 (2008).
- 1317 14. Rousseeuw, P. J. Silhouettes: A graphical aid to the interpretation and validation of
 1318 cluster analysis. *Journal of Computational and Applied Mathematics* 20, 53–65
 1319 (1987).
- 1320
 15. Sherry, S. T., Ward, M. & Sirotkin, K. dbSNP-database for single nucleotide
 polymorphisms and other classes of minor genetic variation. *Genome Research* 9, 677–679 (1999).
- 132316.McKenna, A. *et al.* The Genome Analysis Toolkit: a MapReduce framework for1324analyzing next-generation DNA sequencing data. Genome Research 20, 1297–13251303 (2010).
- 1326 17. Sun, L. *et al.* RNA structure maps across mammalian cellular compartments.
 1327 Nature Structural & Molecular Biology 26, 322–330 (2019).
- 1328 18. Spitale, R. C. *et al.* Structural imprints in vivo decode RNA regulatory 1329 mechanisms. *Nature* **519**, 486–490 (2015).
- 1330 19. Hofacker, I. L. Vienna RNA secondary structure server. *Nucleic Acids Research*1331 31, 3429–3431 (2003).
- 1332 20. Flynn, R. A. *et al.* 7SK-BAF axis controls pervasive transcription at enhancers.
 1333 Nature Structural & Molecular Biology 23, 231–238 (2016).
- 133421.Batista, P. J. *et al.* m6A RNA Modification Controls Cell Fate Transition in1335Mammalian Embryonic Stem Cells. *Cell Stem Cell* 15, 707–719 (2014).
- 1336 1337



bioRxiv preprint doi: https://doi.org/10.1101/667881; this version posted June 11, 2019. The copyright holder for this preprint (which was not certified by peer review) is the author/funder. All rights reserved. No reuse allowed without permission.

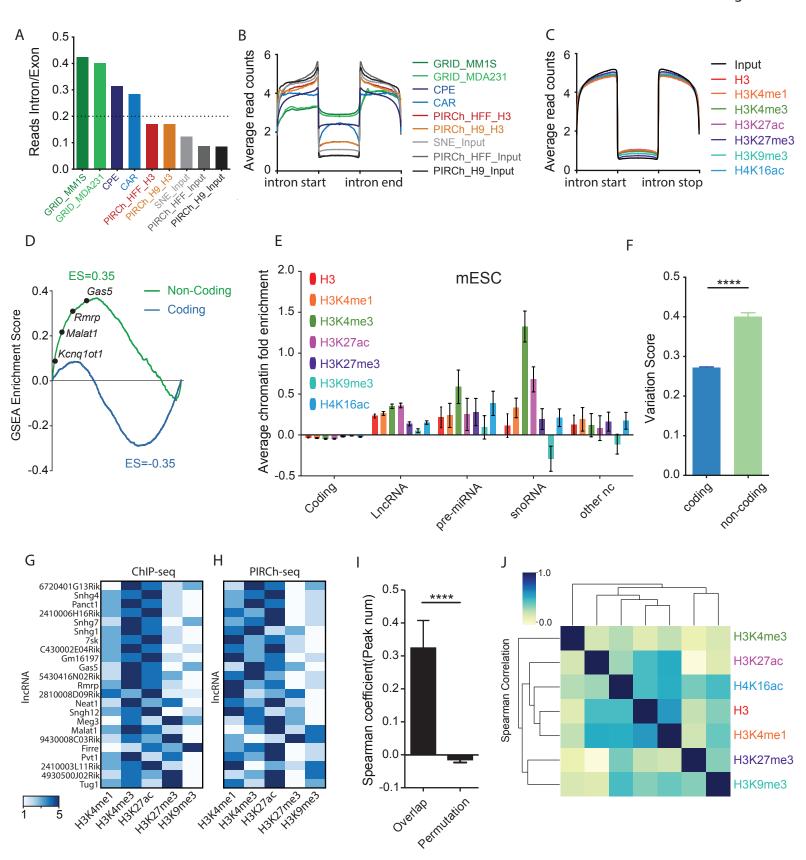
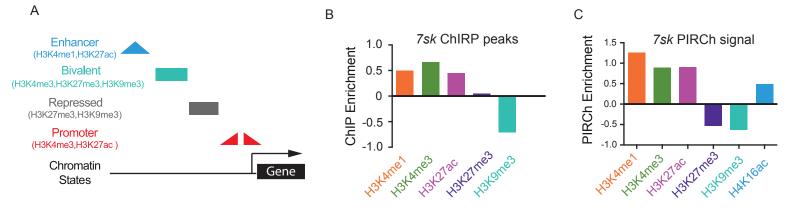
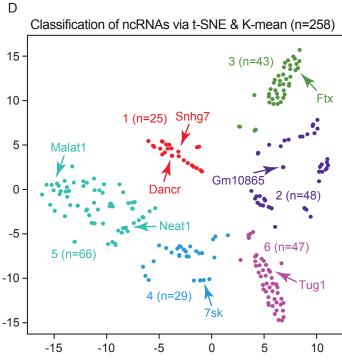
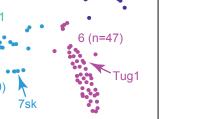


Figure 2



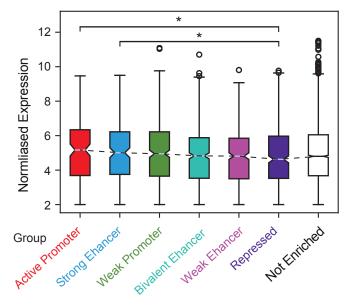
Е





F

Nearby Coding Gene Expression



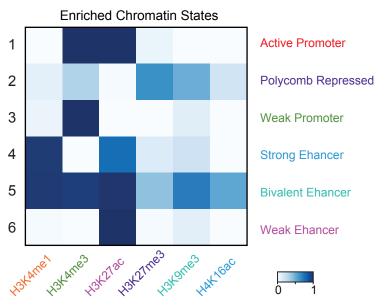
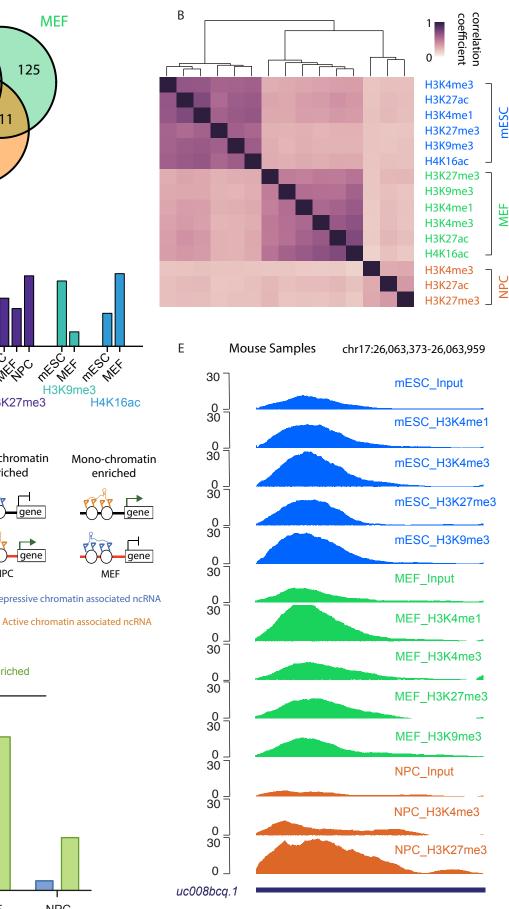
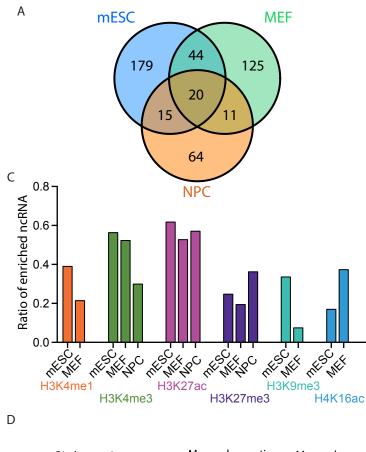
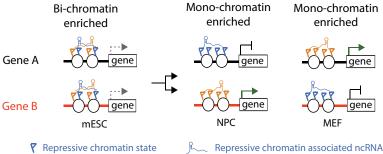


Figure 4







7 Active chromatin state

F

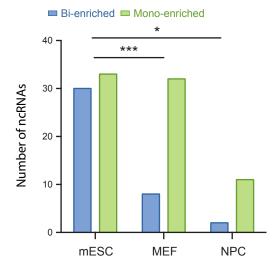
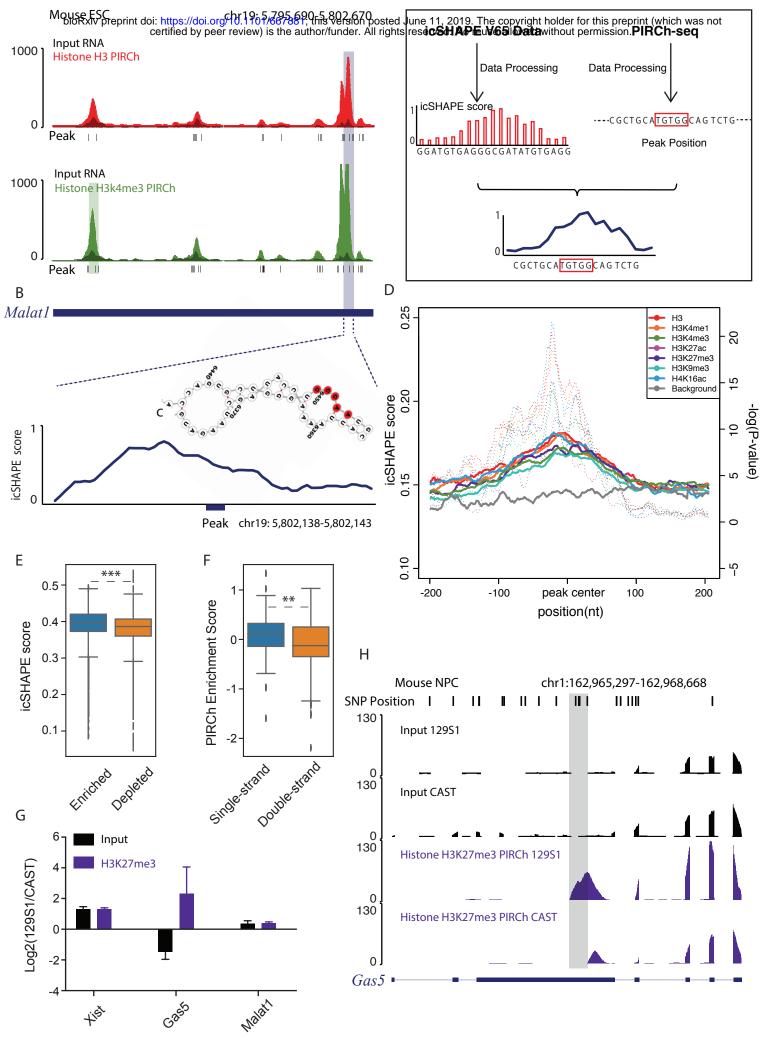
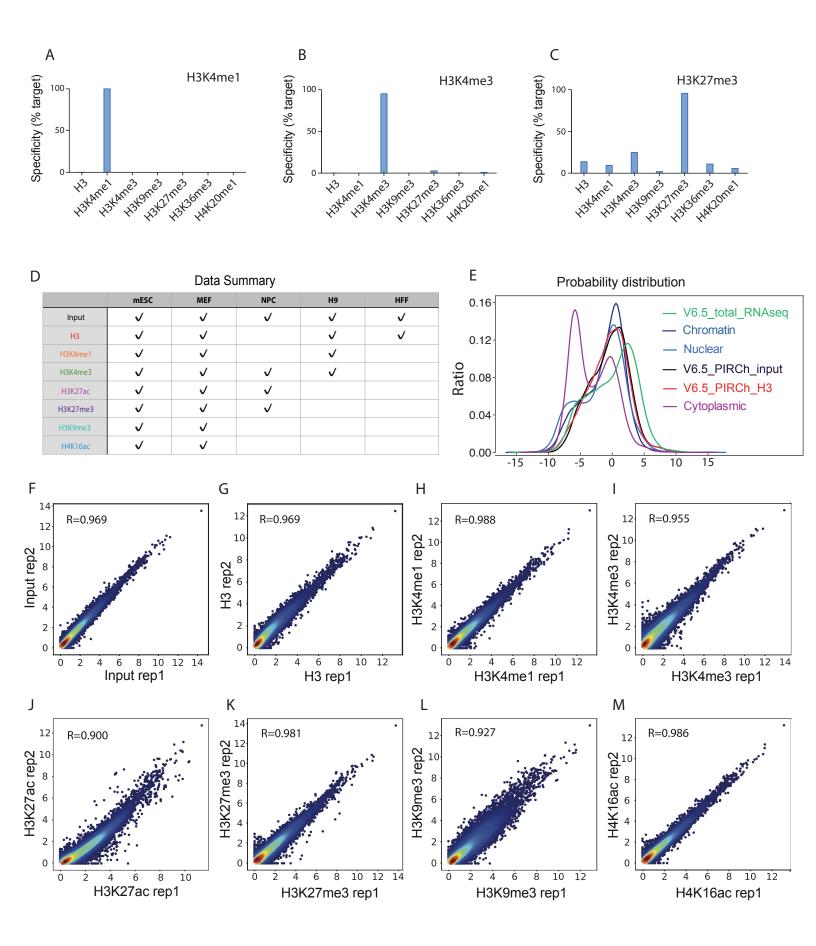




Figure 5

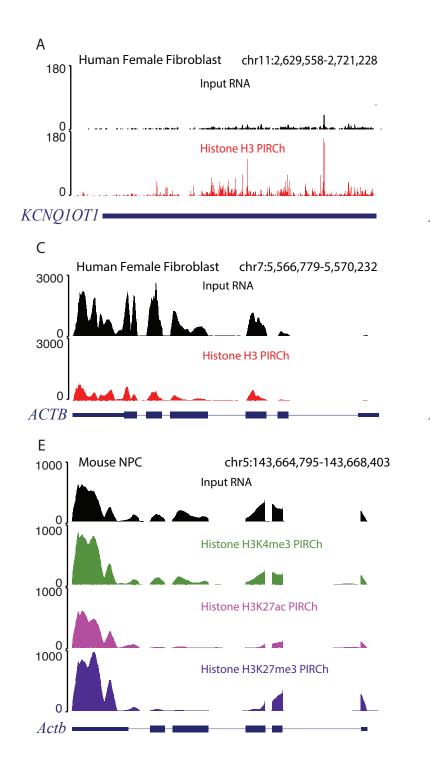


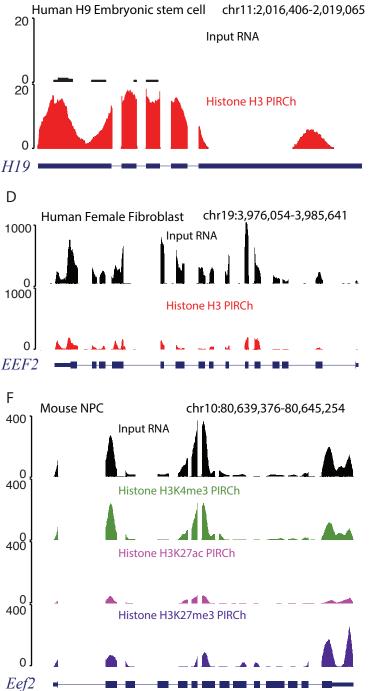
С



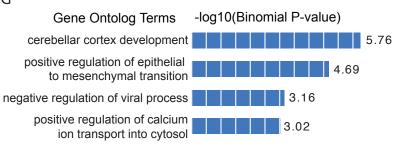
В

Figure S2



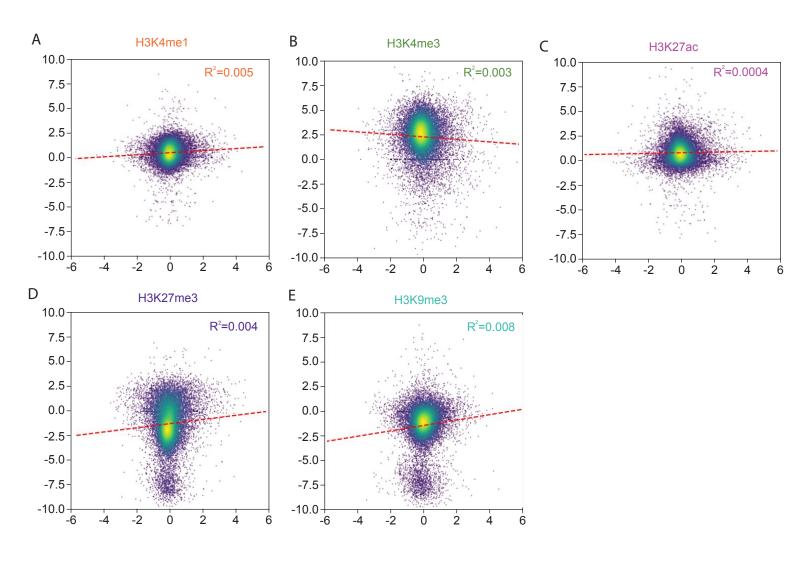


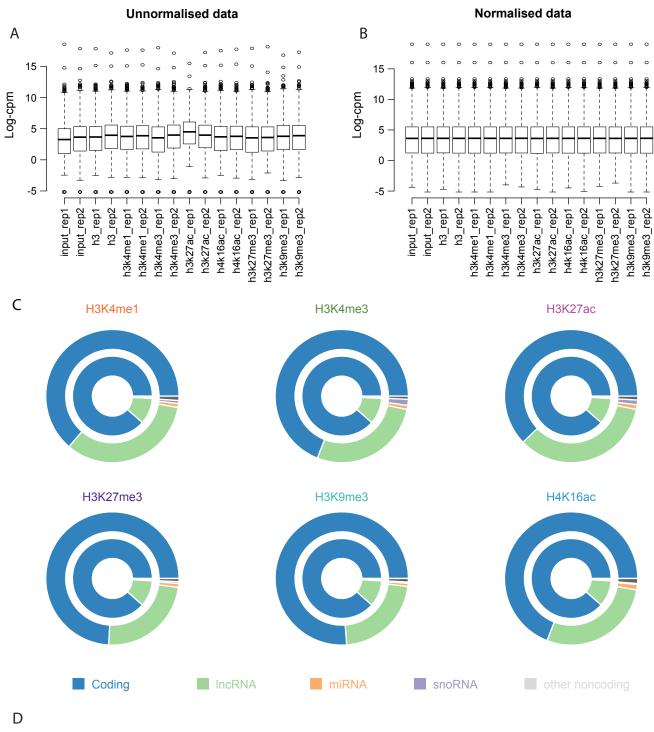
G

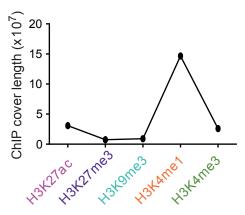


bioRxiv preprint doi: https://doi.org/10.1101/667881; this version posted June 11, 2019. The copyright holder for this preprint (which was not certified by peer review) is the author/funder. All rights reserved. No reuse allowed without permission.

Figure S3







5

4

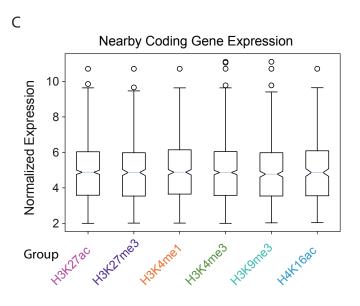
3 2

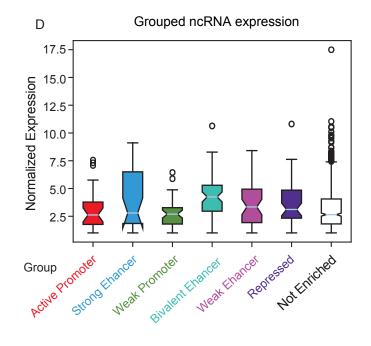
1

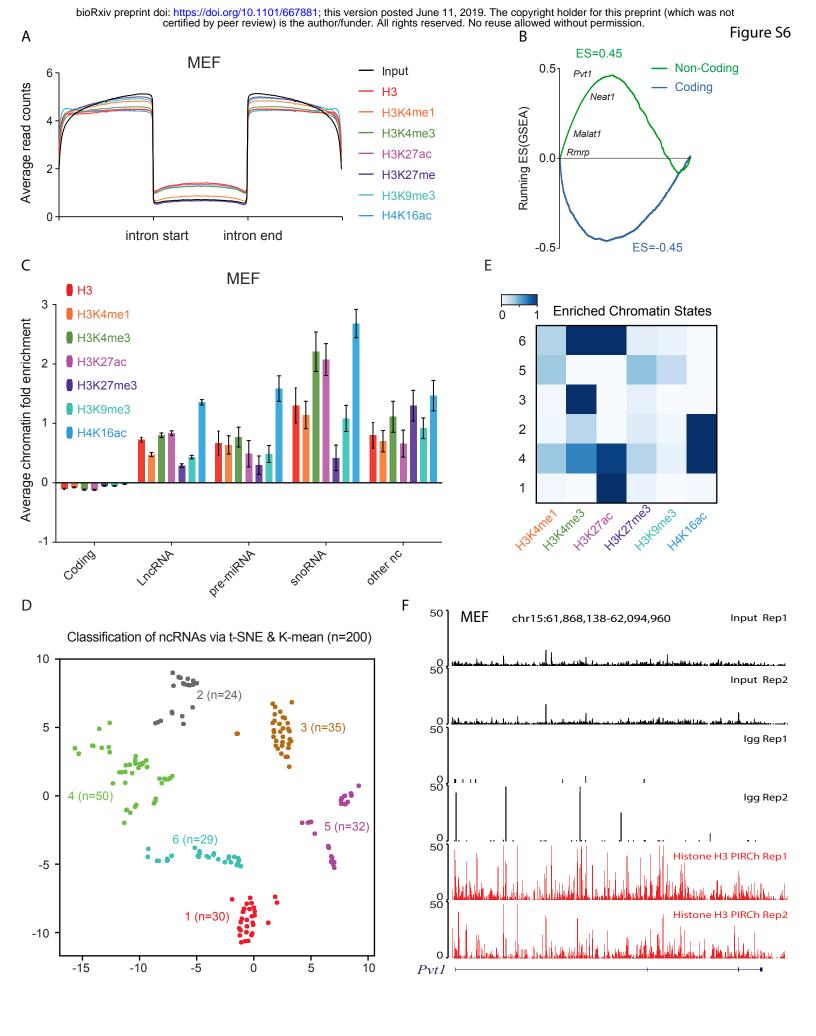
0

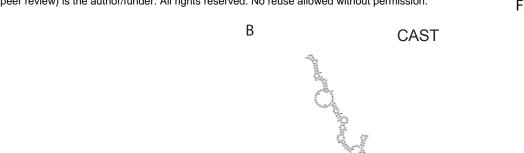
Odds ratio

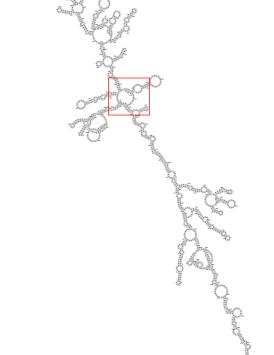
А В 200-LncRNAdb Overlap 150-0 2 0 3 1 Yes 100-41 24 58 44 No Bivalent Enancer Weak Promoter Active Promoter Strong Elencer Repressed WeakEnancer **50**⁻ 0 net H3KAMe3 H3K21ac H3K2Ine3 H3K3me3 HAK16ac Hattamet





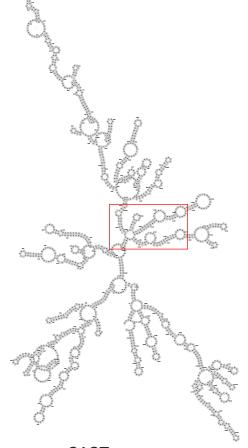




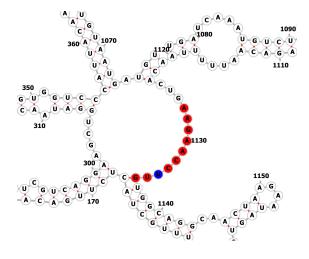


129S1

А

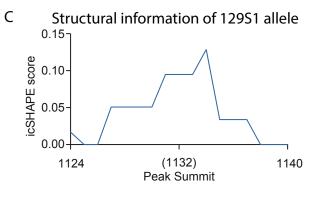


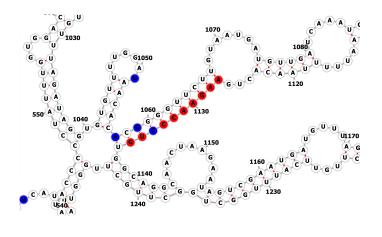




129S1

Peak Position





• SNP Region

bioRxiv preprint doi: https://doi.org/10.1101/667881; this version posted June 11, 2019. The copyright holder for this preprint (which was not certified by peer review) is the author/funder. All rights reserved. No reuse allowed without permission.

